Inhibition of the Notch signal transducer CSL by Pkc53E-mediated phosphorylation to fend off parasitic immune challenge in *Drosophila*

*Sebastian Deichsel[1,#], Lisa Frankenreiter[1], Johannes Fechner[1,§], Bernd M. Gahr[1,+], Mirjam Zimmermann[1], Helena Mastel[1], Irina Preis[1], Anette Preiss[1,&], Anja C. Nagel[1]**

Department of Molecular Genetics, Institute of Biology, University of Hohenheim, 70599 Stuttgart, Germany

now at: Department of Medical Genetics and Applied Genomics, University of Tübingen, 72076 Tübingen, Germany

§ now at: Institute of Biomedical Genetics (IBMG), University of Stuttgart, 70569 Stuttgart, Germany

+ now at: Department of Internal Medicine II, Molecular Cardiology, University of Ulm, 89081 Ulm, Germany

& emerita professor

* Author for correspondence: anja.nagel@uni-hohenheim.de

Key words

CSL, *Drosophila melanogaster*, host defense, immune challenge, Notch inhibition, parasitoid wasp, phosphorylation, Protein Kinase C, Pkc53E, Suppressor of Hairless.

Declaration of interests

The authors declare that no competing interests exist.

Abstract

Notch signalling activity regulates hematopoiesis in *Drosophila* and vertebrates alike. Parasitoid wasp infestation of *Drosophila* larvae, however, requires a timely downregulation of Notch activity to allow the formation of encapsulation-active blood cells. Here we show that the *Drosophila* CSL transcription factor Suppressor of Hairless [Su(H)] is phosphorylated at Serine 269 in response to parasitoid wasp infestation. As this phosphorylation interferes with the DNA-binding of Su(H), it reversibly precludes its activity. Accordingly, phospho-deficient $Su(H)^{S269A}$ mutants are immune compromised. A screen for kinases involved in Su(H) phosphorylation identified Pkc53E, required for normal hematopoiesis as well as for parasitoid immune response. Genetic and molecular interactions support the specificity of the Su(H)-Pkc53E relationship. Moreover, phorbol ester treatment inhibits Su(H) activity *in vivo* and in human cell culture. We conclude that Pkc53E targets Su(H) during parasitic wasp infestation, thereby remodeling the blood cell population required for wasp egg encapsulation.

Introduction

Drosophila melanogaster harbours a sophisticated cellular immune system to fight invaders. The larval hematopoietic system comprises a circulating and sessile compartment of embryonic origin and the developing larval lymph gland, constituting a hematopoietic organ. The circulating and sessile compartment consists primarily of macrophage-like plasmatocytes, plus a small number of crystal cells involved in wound healing and melanization responses to neutralize pathogens. Both cell types differentiate from hemocyte precursors within the lymph gland as well, and they are released during pupal stages to serve the adult with immune cells. Finally, lamellocytes represent the third blood cell type in *Drosophila*. While merely absent in healthy animals, their formation is induced within hours of wasp infestation or wounding (reviewed in: Banerjee et al., 2019; Letourneau et al., 2016; Hultmark and Andó, 2022). In fact, parasitism by endo-parasitoid wasps represents one of the most severe naturally occurring immune challenges to *Drosophila*, invariably causing death if not defended off properly. Parasitoid wasps deposit their egg into the live *Drosophila* larva, where it develops into the next wasp generation egressing from the pupa instead of a fly. Hence, wasp infestation is a life-threatening challenge to the *Drosophila* host, demanding an immediate immune response to overwhelm the parasite. This involves a massive increase in circulating hemocytes, and most energy resources are devoted to fight the invader. Here, lamellocytes play a critical role: they encapsulate the wasp egg and, by expressing Prophenoloxidase, induce a melanization reaction retarding further wasp development (Dudzic et al. 2015; reviewed in: Banerjee et al., 2019; Letourneau et al., 2016; Hultmark and Andó, 2022).

Wasp infestation substantially remodels the composition of the *Drosophila* hemocyte population (Cattenoz et al., 2020; Cho et al., 2020; Tattikota et al., 2020; reviewed in: Csordás et al., 2021). There is a vast increase in plasmatocytes and intermediate precursors in both hematopoietic compartments, from which lamellocyte differentiate. This process requires the combined regulatory input of several pathways, including JAK/STAT, JNK, Toll, Notch, EGFR and INR pathways, which in fact regulate blood cell homeostasis in general (reviewed in Banerjee et al., 2019; Letournau et al., 2018; Csordás et al., 2021). Simultaneous to the massive expansion of lamellocytes, crystal cells are significantly reduced (Crozatier et al., 2004; Krzemien et al., 2010; Ferguson and Martinez-Agosto, 2014; Cattenoz et al., 2020; Cho et al., 2020; Tattikota et al., 2020; reviewed in Csordás et al., 2021). Crystal cells are generated both in the larval lymph gland as well as by trans-differentiation from plasmatocytes in the sessile compartment. Their formation, differentiation and survival strictly depend on Notch signalling activity (reviewed in: Banerjee et al., 2019; Csordás et al., 2021; Hultmark and Andó, 2022).

Lamellocyte and crystal cell lineages are mutually exclusive. Accordingly, while promoting crystal cell fate, Notch activity inhibits differentiation of lamellocytes within the lymph gland, however, is reduced upon wasp infestation (Small et al., 2014). Lamellocyte induction involves the formation and sensing of reactive oxygen species triggered by wasp egg injection (Nappi et al., 1995; Sinenko et al., 2011; Small et al., 2014; Louradour et al., 2017; reviewed in: Banerjee et al., 2019; Csordás et al., 2021). The molecular mechanism underlying the simultaneous crystal cell fate inhibition, however, is less well understood. Obviously, an effective and timely downregulation of Notch activity is required to fend off parasitic wasps.

The Notch pathway is highly conserved between invertebrates and vertebrates, where it regulates numerous cell fate decisions. Notch signals are transduced by CSL type proteins (abbreviation of human CBF1/RBPJ, *Drosophila* Suppressor of Hairless [Su(H)], and worm Lag1), that bind the DNA to direct transcriptional activity of Notch target genes by help of recruited cofactors (reviewed in: Giaimo et al., 2021; Kopan and Ilagan, 2009; Siebel and Lendahl, 2017). In the absence of Notch signals, however, CSL together with corepressors silences Notch target genes, thereby acting as a molecular switch (Borggrefe and Oswald, 2009). Hence, CSL is central to Notch pathway activity as no signal transduction can occur in its absence or in the instance of a lack of DNA-binding. Earlier, we observed Su(H) phosphorylation at Serine 269 in cultured *Drosophila* Schneider S2 cells (Nagel et al., 2017). Of note, Schneider S2 cells have hemocyte characteristics (Cherbas et al., 2011; Schneider, 1972; Terriente-Felix et al., 2013). As a consequence of the negative charge conferred by the phosphorylation at Serine 269, Su(H) loses its affinity to the DNA, and without its DNA-binding ability, also its function as a transcriptional regulator (Nagel et al., 2017). Accordingly, a phospho-mimetic $Su(H)^{S269D}$ mutant behaved like a *Su(H)* loss of function mutant in all respects. In contrast, the phospho-deficient $Su(H)^{S269A}$ variant, appeared wild type at the first glance, indicating some tissue-specificity of this regulatory mechanism. In fact, the $Su(H)^{S269A}$ allele displayed a gain of Notch activity particularly during embryonic and larval hematopoiesis with increased numbers of crystal cells in both hematopoietic compartments (Frankenreiter et al., 2021). Moreover, we found that the general Notch antagonist Hairless is not involved in constraining crystal cell numbers, suggesting that in the context of blood cell homeostasis Notch activity is regulated by the phosphorylation of Su(H) (Maier, 2006; Frankenreiter et al., 2021). As the same set of genes affect blood cell maintenance and differentiation in homeostasis and upon immune challenge (Cho et al., 2020; Tattikota et al., 2020), obviously phospho-mediated downregulation of Notch activity might also occur in response to parasitoid wasp infestation, allowing the formation of encapsulation active lamellocytes at the expense of

82 crystal cells. Briefly, phosphorylation of Su(H) is an elegant mechanism to transiently curb
83 Notch activity in the context of immune responses.
84 In this work, we followed the hypothesis that after wasp infestation, a specific kinase might be
85 activated to phosphorylate Su(H) thereby allowing an adequate immune response. In this case,
86 the phospho-deficient *Su(H)*^{S269A} allele should be immune-compromised, as it cannot respond
87 to phosphorylation, i.e. remaining active even upon parasitism. Indeed, *Su(H)*^{S269A} displayed an
88 increased sensitivity towards parasitoid wasp infestation accompanied by an increase of crystal
89 cells at the expense of lamellocytes. Accordingly, phosphorylation of Su(H) protein was
90 detected in infested wild type larvae but not in the *Su(H)*^{S269A} mutant. In a screen for kinases
91 regulating this process, Pkc53E, the homologue of human PKCα, was identified as an important
92 player. In agreement with a role in blood cell homeostasis, a *Pkc53E*$^{\Delta 28}$ null mutant displayed
93 increased crystal cell numbers. Moreover, genetic and molecular interactions between Su(H)
94 and Pkc53E support the specificity of their relationship. Finally, *Pkc53E*$^{\Delta 28}$ was impaired in its
95 immune response to wasp infestation as well. Together, these data show that Su(H) is a target
96 of Pkc53E during parasitic wasp infestation, inducing phosphorylation and subsequent
97 downregulation of Su(H) activity to allow the mass production of lamellocytes required for
98 wasp defense.

Results

Impaired immune response to parasitoid wasps in the phospho-deficient Su(H)^{S269A} mutant

Wasp infestation alters the course of hematopoiesis, as lamellocyte differentiation is massively increased at the expense of crystal cells. This process requires a timely attenuation of Notch activity that may be implemented by the phosphorylation of Su(H) at Serine 269 (S269). To test this model, we exposed control larvae and larvae of the phospho-deficient *Su(H)^{S269A}* variant to the parasitoid wasp *Leptopilina boulardi* (*L. boulardi*) and analysed the consequences on blood cell homeostasis around 44 hours post-infection, i.e. before lymph gland histolysis. To exclude any influence of the engineered genomic background, we used *Su(H)^{gwt}* for comparison, carrying a genomic wild type construct in place of the mutant (Praxenthaler et al., 2017; Frankenreiter et al., 2021).

Earlier we noted an excess of crystal cells in the phospho-deficient *Su(H)^{S269A}* allele, which we interpret as a gain of Notch activity in consequence of the inability to be downregulated by Su(H) phosphorylation (Frankenreiter et al., 2021) (Figure 1A,B). In agreement with this hypothesis, RNAi-mediated downregulation of *Notch* in hemocytes (*hml*::*N*-RNAi) resulted in a near complete loss of crystal cells. This *Notch* loss of function phenotype was epistatic to the *Su(H)^{S269A}* phenotype, i.e. the excess of crystal cells characterizing *Su(H)^{S269A}* was no longer observed in the combination with *N*-RNAi, demonstrating that Notch acted upstream of Su(H) as expected (Figure 1_ Figure supplement 1). The slightly elevated numbers in the *Su(H)^{S269A}* background compared to the control, however, may be due to the enlarged anlagen in the embryo unaffected by *hml*::*N*-RNAi (Fankenreiter et al., 2021). Total hemocyte numbers were slightly, albeit not significantly increased in *Su(H)^{S269A}* compared to the *Su(H)^{gwt}* control, and correspondingly, hemocyte numbers were somewhat lowered in the *Su(H)^{S269D}* allele (Figure 1_Figure supplement 1). This is in line with earlier observations of unchanged plasmatocyte counts in *N* or *Su(H)* mutants relative to control (Duvic et al., 2002). In response to wasp infestations, however, crystal cell numbers should drop to allow the formation of lamellocytes (Small et al., 2014; Csordás et al., 2021). Indeed in the *Su(H)^{gwt}* control, both the sessile crystal cells as well as those within the larval lymph glands were significantly lessened in response to wasp infestation (Figure 1A,B). In contrast, the higher crystal cell numbers in the *Su(H)^{S269A}* mutant larvae dropped to control-level, demonstrating the impairment of the mutant to detect this immune challenge or to respond to it (Figure 1A,B). Total hemocyte numbers, however, were similar between the genotypes independent of wasp infestation (Figure 1_Figure supplement 1).

133 Increased abundance of lamellocytes upon wasp infestation was monitored *in vivo* in larval
134 hemolymph and lymph glands, using either the L1-*atilla*-GFP reporter (Honti et al., 2009) or
135 *PPO3*-Gal4::UAS-GFP (Dudzic et al., 2015), respectively. In the harvested larval hemolymph
136 of the infested $Su(H)^{gwt}$ control, the hemocytes contained about 15% *PPO3*- and 23% *atilla*-
137 labelled lamellocytes (Figure 1C,D). These numbers were significantly lower in the wasp
138 infested $Su(H)^{S269A}$ larvae (Figure C,D). Consistently, both lamellocyte reporters were robustly
139 induced in the lymph glands of the infested control, but rarely in glands of the $Su(H)^{S269A}$ mutant
140 (Figure 1E,F and Figure1_supplement 2). Obviously, the $Su(H)^{S269A}$ mutant barely responds to
141 the immune challenge raised by the parasitic wasp infestation.
142 In order to monitor the altered immune responses at the molecular level, we quantified Notch
143 target gene expression in the hemolymph upon wasp infestation over time. We observed a
144 decline in the expression of the Notch reporter NRE-GFP immediately after wasp infection in
145 the control $Su(H)^{gwt}$ to about half the value of the uninfected larvae, dropping even further to
146 about 30% 24-30 hours post infection (Figure 1G). $Su(H)^{S269A}$ mutant larvae, however, retained
147 a much stronger expression level at around 60-70% of the uninfected control even at the late
148 time point. These data reveal the downregulation of Notch activity in response to wasp
149 infestation prior or parallel to lamellocyte formation, in agreement with our model, whereby
150 the infestation-induced phosphorylation of Su(H) impairs transmission of Notch signalling
151 activity. Accordingly, the lamellocyte specific marker *atilla* bounced up nearly two magnitudes
152 in the wasp infected $Su(H)^{gwt}$ control at the late time point, but not in $Su(H)^{S269A}$ compared to
153 the uninfected control (Figure 1G) (Cattenoz et al., 2020).
154 Overall, these data support the model that S269 in Su(H) is a molecular target for a kinase,
155 phosphorylated upon immune challenge to allow lamellocyte formation at the expense of
156 crystal cells.
157
158 ***The phospho-deficient $Su(H)^{S269A}$ allele is impaired in combating wasp infestation***
159 Parasitoid wasp infestation constitutes an extreme immune challenge for the *Drosophila* larva:
160 if not combatted by the immune system, a wasp egg, which is deposited in the larval body
161 cavity, will develop into an adult wasp, thereby killing the larval host during the pupal stage.
162 Indeed, depending on the wasp species used, we measured a high mortality rate with less than
163 5% up to about 14% of surviving flies, whereas nearly all pupae hatched to adults without wasp
164 challenge (Figure 2A). According to our working hypothesis, the phospho-deficient $Su(H)^{S269A}$
165 variant should not be able to properly respond to the immune challenge. To test this directly,

166 we measured the survival of *Su(H)*^{S269A} animals upon wasp infestation compared to the wild
167 type control.
168 The two closely related wasp species *L. boulardi* and *Leptopilina heterotoma* (*L. heterotoma*)
169 very efficiently parasitized both the control *Su(H)*^{gwt} and the *Su(H)*^{S269A} variant, though the latter
170 appeared slightly more sensitive (Figure 2A). The difference in mortality became more apparent
171 with the wasp species *Asobara japonica* (*A. japonica*), allowing 14% of the *Su(H)*^{gwt} control
172 flies to escape parasitism, whereas only 3.4% of the infested *Su(H)*^{S269A} pupae emerged as flies.
173 Thus, the *Su(H)*^{S269A} mutants are less robust in resisting parasitoid wasp infestation consistent
174 with an impaired immune response.
175
176 ***Serine 269 of Su(H) is phosphorylated upon wasp infestation***
177 Next, we wanted to directly monitor Su(H) phosphorylation at S269 in response to wasp
178 infestation. To this end, polyclonal antibodies directed against a phosphorylated peptide
179 containing the sequence motif NRLRpSQTVSTRYLHVE were generated (α-pS269).
180 Specificity was first tested by Western blot analysis using bacterially expressed GST fusion
181 proteins containing the entire beta-trefoil domain (BTD) of Su(H), as well as with phospho-
182 mimetic (S269D) and phospho-mutant (S269A) versions. All three variants were detected by
183 the antisera. The S269D version, however, was strongly preferred, indicating that this antibody
184 does preferably recognize phospho-S269 Su(H) protein (Figure 2 - Figure supplement 1).
185 Encouraged by this result, we used this antiserum on protein extracts derived from larvae
186 infested and not infested by *L. boudardi*. For this experiment we used genome engineered fly
187 strains expressing mCherry-tagged Su(H) proteins, *Su(H)*$^{S269A\text{-}mCh}$ and *Su(H)*$^{gwt\text{-}mCh}$ for control
188 (Praxenthaler et al., 2017). Su(H) proteins were trapped using RFP-nanobody coupled agarose
189 beads, and the precipitates were then probed in Western blots with antibodies directed against
190 mCherry and pS269. Indeed, α-pS269 antibodies recognized Su(H)$^{gwt\text{-}mCh}$ protein in wasp
191 infested larvae, indicating respective phosphorylation of Su(H) protein. No such signals were
192 seen in precipitates from the non-infected larvae nor from any of the *Su(H)*$^{S269A\text{-}mCh}$ mutant
193 larvae (Figure 2B). These data strongly support the notion of parasitism-induced
194 phosphorylation of Su(H) at S269. Apparently, parasitoid wasp infestation starts a cascade of
195 events resulting in the inhibitory S269 phosphorylation of Su(H) protein to allow lamellocyte
196 formation. Hence, the question arose on the kinase/s involved in this process.
197
198 ***Screening of kinase candidates mediating phosphorylation of Su(H) at Serine 269***

199 To identify Ser/Thr kinases involved in the phosphorylation of Su(H) at S269, we commenced
200 with a combination of *in silico* and biochemical approaches aiming to generate a list of
201 candidate kinases which can be further analysed by genetic means (Figure 3). First, by using
202 GPS 3.0 software that encompasses a substantial database of kinases and their preferred
203 recognition motives (Xue et al., 2011), 36 potential human kinases were predicted to recognize
204 S269 as substrate, represented by 30 kinases in *Drosophila* (Figure 3 –Table 1 supplement). In
205 addition, the BTD domain of Su(H) was bacterially expressed as a GST fusion protein and
206 subjected to phospho-assays using 245 different human Ser/Thr kinases. Our reasoning for
207 using the entire BTD domain was to ensure a normal folding of the domain (Kovall and
208 Blacklow, 2010), and to reduce the number of potential phospho-sites at the same time present
209 in full length Su(H). With this approach, we ended up with 62 human Ser/Thr kinases (25% of
210 the tested kinases) that use the BTD of Su(H) as an *in vitro* substrate, corresponding to 40
211 different kinases in *Drosophila* (Figure 3–Table 2 supplement). Both sets of data, biochemical
212 and bioinformatics, were used to generate a list of 44 candidates to be analysed by genetic
213 means. The candidates were further screened for an imbalanced hematopoiesis. We reasoned
214 that mutants affecting a relevant kinase gene involved in the phosphorylation of Su(H) should
215 display increased crystal cell numbers similar to what was observed in the $Su(H)^{S269A}$ mutant
216 (Frankenreiter et al., 2021). Larvae of 13 different kinase mutants, and the progeny of 44 UAS-
217 RNAi and/or UAS-kinase dead transgenes crossed with *hml*-Gal4, a blood cell-specific Gal4
218 driver line, were tested (Figure 3 –Table 3 supplement). To this end, the larvae were subjected
219 to heating for a visualization and quantification of sessile crystal cells (Rizki, 1957; Lanot et
220 al., 2001). About a third of the kinase mutants were similar to the control, whereas mutations
221 in four kinases impeded crystal cell development or prevented it altogether. Unexpectedly, the
222 majority of the tested kinase mutants exhibited elevated crystal cell numbers, however to a
223 different degree (Figure 3_Figure supplement 1, Table 4 supplement) (Deichsel et al., 2024).
224 Nineteen kinase mutants matched closely the $Su(H)^{S269A}$ phenotype, making those the most
225 promising candidates to being involved in the phosphorylation of Su(H) at S^{269}. Six of those
226 were within the cluster of ten candidates singled out by the *in silico* and the *in vitro* screens
227 (Figure 3 A,B). Using commercially available, activated human kinases, we were able to test
228 five candidates, AKT1, CAMK2D, GSK3B, S6 and PKCα in vitro by MS/MS analysis on the
229 Su(H) peptide ALFNRLR$\mathbf{S}^{8}$QTVSTRY, where Serine 8 (S8) corresponds to S269 in Su(H).
230 Only PKCα unambiguously phosphorylated the given peptide at Serine 8. Whereas GSK3B did
231 not phosphorylate the peptide at all, AKT1, CAMK2D and S6 piloted Threonine 10,
232 corresponding to Threonine 271 in Su(H) (Figure 3D, Figure 3_Figure supplement 2). Together,

233 these data support the idea, that PKCα corresponding to Pkc53E in *Drosophila*, is part of the
234 kinase network mediating the phosphorylation of Su(H) at S269.
235
236 ***Role of Pkc53E in the phosphorylation of Su(H)^{S269}***
237 Confirming the MS/MS data, human PKCα was able to phosphorylate the respective Su(H)
238 peptide (S^{wt}) similar to its defined pseudo-substrate PS (Kochs et al., 1993), whereas the S8A
239 mutant peptide (S^{SA}) was accepted only half as well in an ADP-Glo^{TM} assay, indicating that
240 S269 is a preferred substrate (Figure 4A). Bacterially expressed and purified *Drosophila*
241 Pkc53E, however, did neither accept the PS nor the Su(H) peptides (Figure 4B). Pkc53E
242 activity, however, was stimulated by the agonistic phorbol ester PMA (phorbol 12-myristate
243 13-acetate) (Blumberg et al., 1983; Nakashima, 2002) to phosphorylate the PS and Su(H)
244 peptide S^{wt} but not the S8A mutant peptide S^{SA} (Figure 4C). To generate an activated form of
245 Pkc53E, we exchanged four codons by *in vitro* mutagenesis, three (T508D, T650D and S669D)
246 mimicking phosphorylation in the kinase and C-terminal domains, respectively, and one in the
247 pseudo-substrate domain (A34E) (Figure 4_Figure supplement 1) (Gould and Newton, 2008).
248 The resultant Pkc53E^{EDDD} kinase accepted the PS, and the Su(H) peptide S^{wt} even better, but
249 not the S8A mutant peptide S^{SA}, demonstrating the specificity of the phosphorylation (Figure
250 4D). As predicted for a fully activated kinase, PMA was unable to boost Pkc53E^{EDDD} protein
251 activity any further (Figure 4E). The bacterially expressed Pkc53E^{EDDD} kinase, however, was a
252 magnitude less active compared to commercial PKCα, perhaps reflecting poor quality of the
253 bacterially expressed protein, or indeed an intrinsic biochemical property of the *Drosophila*
254 enzyme.
255
256 ***The PKC-agonist PMA influences Su(H) activity and blood cell homeostasis***
257 Our data so far indicated that Su(H) is a phospho-target of Pkc53E which reduces its activity
258 by affecting its DNA-binding. In this case, we might expect an influence of the general PKC-
259 activator PMA on both, Su(H) activity as well as Notch-mediated crystal cell formation. We
260 tested the former in a *RBPJ^{ko}* HeLa cell system (Wolf et al., 2019), measuring Notch-reporter
261 gene activation by Su(H)-VP16. To this end, a Su(H)-VP16 gene fusion was cloned under HSV-
262 TK promoter control, which is unresponsive to PMA in HeLa cells (Shifera and Hardin, 2009).
263 Su(H)-VP16 protein is independent of Notch activity itself, allowing to directly monitor the
264 influence of PMA on Su(H) activity. Indeed, Su(H)-VP16 ability to activate reporter gene
265 transcription was reduced by more than half in the presence of PMA (Figure 5A). This is in
266 agreement with a PMA-mediated activation of endogenous PKC in the transfected HeLa cells,

267 resulting in Su(H)-VP16 phosphorylation, loss of DNA-binding activity and reduced
268 transcriptional activation. Accordingly, repression could be reverted by the addition of kinase-
269 inhibitor Staurosporine (Karaman et al., 2008). In fact, Staurosporine alone already increased
270 Su(H)-VP16 transcriptional activity, suggesting that inhibitory phosphorylation of Su(H)
271 occurs in HeLa cells (Figure 5A). Expression levels of Su(H)-VP16, however, remained
272 unchanged by the treatments (Figure 5_Figure supplement 1).
273 Next, we assayed the effect of PMA on larval crystal cell formation. If, as expected, PMA
274 increased Pkc53E activity, Su(H) should be inactivated by phosphorylation with decreased
275 crystal cell numbers as a consequence. We fed PMA to *Drosophila* larvae and assayed the
276 numbers of sessile crystal cells. In agreement with our expectations, crystal cell numbers
277 dropped very strongly, suggesting efficient phosphorylation and inactivation of Su(H) protein
278 by PKCs (Figure 5B). As predicted by the above experiments, this effect was alleviated by
279 Staurosporine. Owing to the global inhibition of kinases by Staurosporine, however, a rise in
280 crystal cells was expected, because many kinases restrict their numbers (see Figure 3_Figure
281 supplement 1) (Deichsel et al., 2024). In contrast, $Su(H)^{S269A}$ mutant larvae displayed an
282 increased number of crystal cells which can be attributed to the fact that here, Su(H) can no
283 longer be phosphorylated and hence, is overactive in this context. Feeding PMA to $Su(H)^{S269A}$
284 larvae caused only a minor drop of excessive crystal cell numbers, which could be due to other
285 kinases acting on $Su(H)^{S269}$ or due to other Pkc53E substrates involved in crystal cell
286 development. Again, kinase inhibition by Staurosporine largely reversed this effect (Figure 5B).
287 In conclusion these data support the notion that Su(H) activity is regulated *in vitro* and *in vivo*
288 by PKC activity in the context of blood cell homeostasis.
289
290 ***Pkc53E is required for normal blood cell homeostasis in Drosophila larvae***
291 $Su(H)^{S269A}$ mutant larvae develop an excess of crystal cells, both in the hemolymph as well as
292 in the lymph glands, due to a failure to downregulate respective Notch activity in the particular
293 progenitor cells via the phosphorylation of Su(H) protein (Frankenreiter et al., 2021) (see Figure
294 1A,B). Assuming Pkc53E has a major role in the phosphorylation of Su(H), we should expect
295 a similar phenotype in a *Pkc53E* mutant due to the inability to phosphorylate any substrate. In
296 order to test this assumption directly, we assessed the number of crystal cells in larval lymph
297 glands as well as in sessile crystal cells in several loss of function backgrounds of *Pkc53E*. To
298 this end, we used the $Pkc53E^{\Delta 28}$ allele, which by RT-PCR is a null mutant (Figure 6 – Figure
299 supplement 1). In addition, we used two different RNAi-lines and one sgRNA line under UAS-
300 control to knockdown *Pkc53E* activity specifically in progenitor cells within the developing

301 lymph gland using *lz*-Gal4 and in the hemolymph using *hml*-Gal4, respectively (Lebestky et
302 al., 2000). As the *hml*-Gal4 driver is active in plasmatocytes and pre-crystal cells (Mukherjee
303 et al., 2011; Tattikota et al., 2020), it should affect *Pkc53E* activity prior to crystal cell
304 commitment in the hemolymph. However, within the lymph gland, *hml* appears specific to the
305 plasmatocyte lineage and not present in crystal cell precursors. Instead, we choose *lz*-Gal4 for
306 the *Pkc53E* knockdown, as *lz* is expressed in differentiating crystal cells of the lymph gland
307 (Lebetsky et al., 2000; Blanco-Obregon et al., 2020).
308 In any context tested, the number of crystal cells was strongly increased matching those of the
309 $Su(H)^{S269A}$ mutant (Figure 6, Figure 6_supplement 2). The similar phenotypes imply that
310 Pkc53E acts through the phosphorylation of Su(H) specifically within hemocytes to restrict
311 crystal cell differentiation. However, as outlined above, the majority of kinase mutants
312 displayed increased crystal cell numbers, raising the possibility of a fortuitous accordance. If
313 the increase of crystal cell numbers in *Pkc53E* mutants is independent of Su(H)
314 phosphorylation, we should expect an additive effect if we combine the two mutants. The
315 double mutants $Su(H)^{S269A}$ $Pkc53E^{\Delta 28}$ were generated by genetic recombination; they displayed
316 the same range of excessive crystal cell numbers as the single mutants (Figure 7A,B, Figure
317 7_supplement 1). Moreover, the strongly reduced number of crystal cells observed in the
318 $Su(H)^{S269D}$ mutant was not increased by $Pkc53E^{\Delta 28}$ (Figure 7A,B), indicating that Pkc53E
319 indeed acts upstream of Su(H), or directly on Su(H). If the latter is the case, we may expect the
320 two proteins to form complexes *in vivo*. Indeed, we could co-precipitate Su(H)-Pkc53E protein
321 complexes, both from *Drosophila* heads containing hemocytes (Sanchez Bosch et al., 2019), as
322 well as from the larval hemolymph (Figure 7C,D). Specific co-precipitation was eased by using
323 fly strains expressing m-Cherry tagged Su(H) (Praxenthaler et al., 2017) and HA-tagged
324 Pkc53E, respectively. Together, these data demonstrate that *Pkc53E* has an important role in
325 blood cell homeostasis that can be largely explained by its activity to phosphorylate Su(H),
326 thereby regulating the activity of Notch target genes during hemocyte and lymph gland
327 development.
328
329 ***Pkc53E mutants are immune compromised***
330 According to our hypothesis, Pkc53E phosphorylates Su(H) in response to an immune
331 challenge by parasitic wasp infestation. In fact, a Pkc53E-eGFP fusion protein expressed from
332 the *Pkc53E* locus via protein trap (Lee et al., 2018) was observed in the cytoplasm of all blood
333 cell types independent of wasp infestation (Figure 8). Moreover, *Pkc53E* mRNA was expressed
334 in cells of the larval hemolymph (Figure 8_supplement S1). Hence, we would expect that a loss

335 of Pkc53E function should affect the ability of *Drosophila* larvae to fight wasp infestations
336 similarly to the *Su(H)*^{S269A} mutant. This was indeed the case. Firstly, the *Pkc53E*$^{\Delta 28}$ null mutant
337 was likewise impaired in fighting an infestation with the wasp *A. japonica* as was the *Su(H)*^{S269A}
338 mutant or the double mutant *Su(H)*^{S269A} *Pkc53E*$^{\Delta 28}$ with only about 4% surviving flies versus
339 14% in the control (Figure 9A). In contrast to *Su(H)*^{S269A}, however, the *Pkc53E*$^{\Delta 28}$ mutant larvae
340 contained significantly lower hemocyte numbers independent of infestation, perhaps partly
341 explaining the poor immune response (Figure 9_supplement S1) (McGonigle et al., 2022).
342 Without infestation, however, *Pkc53E*$^{\Delta 28}$ mutant larvae developed normally to adulthood
343 (Figure 9_supplement S1). Moreover, when *Pkc53E*$^{\Delta 28}$ was infested with the parasitic wasp *L.*
344 *boulardi*, lamellocyte numbers in the hemolymph did not reach wild type levels, and they were
345 almost absent from the larval lymph glands (Figure 9B,C). Apparently, the *Pkc53E*$^{\Delta 28}$ null
346 mutant is impaired in recognizing parasitic wasp infestation or is hampered responding to it,
347 for example by the phosphorylation of Su(H), demonstrating the involvement of this kinase in
348 the immune response of *Drosophila* to parasitoid wasp infestation.

349

350 **Discussion**

351

352 The Notch pathway is highly conserved between invertebrates and vertebrates, with regard to
353 both the underlying molecular principles as well as the biological processes it is involved,
354 including hematopoiesis and immune defence. During mammalian hematopoiesis, Notch plays
355 a fundamental role in stem cell maintenance and proliferation as well as in the differentiation
356 of blood cell precursors, notably in T-cell development. Accordingly, aberrant Notch signalling
357 activity has profound consequences for blood cell homeostasis that may result in leukemia
358 (reviewed in: Radtke et al., 2010; Siebel and Lendahl, 2017; Banerjee et al., 2019; Gallenstein
359 et al., 2023). Hence, the principles of the regulation of Notch signalling activity are of great
360 interest.
361 Notch signals are transduced by CSL-type DNA-binding proteins that are pivotal to Notch
362 pathway activity, as no signal transduction could occur in their absence or in the instance of a
363 lack of DNA-binding. CSL proteins are extremely well conserved. They act as a molecular
364 switch, either activating or repressing Notch target genes, depending on the recruited cofactors.
365 Upon ligand binding, the Notch receptor is cleaved, and the biologically active Notch
366 intracellular domain assembles an activator complex with CSL and further co-factors. In the
367 absence of Notch receptor activation, however, CSL recruits co-repressors for gene silencing;
368 in *Drosophila* repressor complex formation is mediated by Hairless (reviewed in: Maier, 2006;
369 Borggrefe and Oswald, 2009; Kovall and Blacklow, 2010; Bray, 2016; Giaimo et al., 2021).
370 Accordingly, a loss of DNA-binding by CSL is expected to affect both, the activation of Notch
371 targets in the presence, as well as their repression in the absence of Notch signals. This dual
372 effect was observed the context of wing development in cells homozygous for the DNA-binding
373 defective $Su(H)^{S269D}$ variant: a failure of Notch target gene expression in areas of high Notch
374 activity, as well as a de-repression of Notch target genes in areas outside (Frankenreiter et al.,
375 2021). Phosphorylation of Su(H) hence entails not only the inhibition of Notch activity, but
376 likewise a de-regulation of genes silenced by Su(H)-repressor complexes. Previously, we have
377 shown that the regulation of Notch activity during hemocyte differentiation is independent of
378 Hairless, but rather relies on the phosphorylation of Su(H) (Frankenreiter et al., 2021).
379 Moreover, Notch activity needs to be downregulated before lamellocyte formation during
380 parasitism, arguing for an inhibition of Notch activity rather than a de-repression of Notch target
381 genes resulting from Su(H) phosphorylation during wasp parasitism.

382 Studies of *Drosophila* hematopoiesis have uncovered a pleiotropic role of Notch in all the
383 hematopoietic compartments, where Notch activity needs to be precisely regulated to ensure
384 blood cell homeostasis (reviewed in: Banerjee et al., 2019; Csordás et al., 2021). During blood
385 cell formation, Notch directs the crystal cell lineage. Accordingly, a downregulation of Notch
386 activity causes a loss of crystal cells, whereas a gain of Notch activity results in increased
387 numbers (Duvic et al., 2002; Lebestky et al., 2003; Terriente-Felix et al., 2013; Gosh et al.,
388 2015; Frankenreiter et al., 2021). In our earlier work, we have shown that the phosphorylation
389 at S269 in the beta-trefoil domain of Su(H) impairs DNA-binding activity, and hence the
390 capability of Su(H) to act as a transcriptional regulator in the context of blood cell development,
391 without affecting Su(H) protein expression (Nagel et al., 2017; Frankenreiter et al., 2021).
392 Accordingly, phospho-deficient $Su(H)^{S269A}$ mutants develop an excess of crystal cells. Now we
393 provide evidence that Su(H) phosphorylation is likewise involved in parasitoid wasp defense,
394 pointing to a dual use of the Notch pathway in blood cell homeostasis as well as in stress
395 response, which is typical for the myeloid system (Banerjee et al., 2019).
396 The primary cellular immune response of *Drosophila* to fight parasitoid wasp infestation is an
397 encapsulation of the parasite egg to terminate its further development. Albeit metabolically
398 extremely costly, *Drosophila* larvae have to remodel their entire hematopoietic system to
399 generate the masses of lamellocytes required for the encapsulation (reviewed in Letournau et
400 al., 2016; Kim-Jo et al., 2019; Csordás et al., 2021; Hultmark & Andó, 2022). There are two
401 major sources for the lamellocytes. One is the transdifferentiation of circulating plasmatocytes,
402 released from the sessile compartment and proliferating upon immune challenge (Márkus et al.,
403 2009; Honti et al., 2010; Stofanko et al., 2010; Vanha-Aho et al., 2015; Anderl et al., 2016).
404 Second is a massive expansion of prohemocytes in the lymph gland followed by a
405 differentiation to lamellocytes and their release due to the premature disintegration of the gland
406 (Lanot et al., 2001, Sorrentino et al., 2002, Louradour et al., 2017; Cho et al., 2020). Wasp
407 infestation hence provokes a biased commitment to the lamellocyte lineage at the expense of
408 crystal cells, as the two lineages are mutually exclusive (Krzemien et al., 2010; Tattikota et al.,
409 2020; Cho et al., 2020; Cattenoz et al., 2020).
410 The processes underlying the *Drosophila* immune response to wasp parasitism are well-
411 understood, sharing many molecular details with the inflammatory responses of vertebrates
412 (reviewed in Letourneau et al., 2016; Kim-Jo et al., 2019; Banerjee et al., 2019; Kharrat et al.,
413 2022). Interestingly, sterile injury of *Drosophila* larvae initiates a likewise immune response
414 covering all aspects of wasp-mediated immune challenge (Evans et al., 2022). The epidermal
415 penetration by the wasp ovipositor causes a burst of hydrogen peroxide at the injury site via the

416 activation of the NADPH oxidase DUOX. The oxidative stress then induces a systemic
417 activation of Toll/NF-κB and JNK-signalling within circulating hemocytes as well as within
418 the cells of the posterior signalling center of the lymph gland. Following cytokine release,
419 JAK/STAT and EGFR signalling pathways are activated non-cell autonomously driving the
420 (trans-)differentiation of (pro-)hemocytes to lamellocyte fate and lymph gland dispersal (Nappi
421 et al., 1995; Schlenke et al., 2007; Sinenko et al., 2011; Gueguen et al., 2013; Razzell et al.,
422 2013; Louradour et al., 2017; Chakrabarti and Visweswariah, 2020; Evans et al., 2022;
423 reviewed in Letourneau et al., 2016; Banerjee et al., 2019). Whereas the switch to lamellocyte
424 fate is well elaborated, less is known about the processes underlying the simultaneous
425 suppression of crystal cell fate. Obviously, this step requires a downregulation of Notch
426 signalling activity, as the Notch pathway is instrumental to crystal cell fate in all the
427 hematopoietic compartments (Duvic et al., 2002; Lebestky et al., 2003; Schlenke et al., 2007;
428 Small et al., 2014; reviewed in Banerjee et al., 2019). Our work now reveals that a parasitoid
429 wasp attack causes a phosphorylation of Su(H) on S269 as means of an efficient and reversible
430 way to inhibit Notch activity. This idea is consistent with earlier observations, whereby wasp
431 parasitism quenched the expression of a Su(H)-lacZ reporter (Small et al., 2014). Moreover, we
432 provide evidence that Pkc53E is involved in Su(H) phosphorylation during blood cell
433 development as well as during parasitoid wasp-defense in *Drosophila*. Moreover, the
434 involvement of PKCs in wasp defense is not completely unexpected given their well-
435 documented role in the immune responses of mammals and *Drosophila* alike. For example,
436 *Drosophila* flies ensure a healthy gut-microbiota homeostasis by modulating DUOX activity as
437 a pathogen-specific defense line (reviewed in Kim and Lee, 2014). DUOX activation and ROS
438 production, induced by gut pathogens was shown to be mediated by Pkc53E and Ca^{2+} via
439 phospholipase Cβ (Ha et al., 2009; Lee et al., 2015). Sterile wounding of the *Drosophila* embryo
440 triggers an instantaneous Ca^{2+} flash followed by hydrogen peroxide production (Razzel et al.,
441 2013). It is conceivable that the epidermal breach by the wasp's sting similarly induces a Ca^{2+}
442 flash that may spark Pkc53E activation as a result. However, PKCs may be activated directly
443 by oxidative modification even in the absence of Ca^{2+}. Moreover, they may promote
444 endogenous ROS production in a positive feedback loop (reviewed in Cosentino-Gomes et al.,
445 2012), that could support the systemic response in the larval lymph gland.
446 The role of PKCs in the mammalian hematopoietic and immune systems is well documented.
447 PKCs in this context act redundantly, and presumably, this holds also true for *Drosophila* where
448 several PKCs exist. Upon activation, PKCs may translocate into the nuclear compartment,
449 where they can directly influence gene expression programs, for example by piloting chromatin

factors as substrates, pivotal for regulating immune cell differentiation (reviewed in Lim et al., 2015). Whereas *Drosophila* Pkc53E appears primarily cytoplasmic, its nuclear presence in some hemocytes is consistent with acting directly on Su(H) once activated (Figure 8A). Phosphorylation, however, may occur also at the membrane or in the cytoplasm, since Su(H) is imported into the nucleus together with its co-regulators (Wolf et al., 2019). PKCs, including PKCα, are present in CD34+ long-term hematopoietic stem cells. Moreover, specific roles in both the myeloid and the multilymphoid lineages are known. Notably, some PKC isoforms including PKCα may play a role in Notch-dependent T-cell development. Notch pathway activity is indispensable for T-cell lineage commitment of early thymic progenitors, however, is rapidly downregulated after the β-selection phase. As treatment with phorbol ester upregulates the transcription of TCRα and β chains, a role of PKC in Notch-dependent commitment of αβ T-cells has been proposed (reviewed in Altman and Kong, 2016; Yui and Rothenberg, 2014). During initial T-cell development, Notch1 signalling increases in intensity, however,is abruptly downregulated at the transcriptional level following β-selection. This rapid downregulation is mediated by the inhibition of the E proteins (Yashiro-Ohtani et al., 2009), however, might in addition involve the phosphorylation of CSL by PKCα. Cell fate in more mature thymocytes is then fixed by the silencing of Notch target genes through chromatin modulators (reviewed in Yui and Rothenberg, 2014).

Appropriate silencing of Notch signalling activity in the course of T-cell development is of utmost importance, as prolonged Notch activity during β-selection predisposes the T-cells to leukemic transformation. Phosphorylation of CSL proteins by PKCα kinase offers a way for a timely and reversible deactivation of Notch signals not only in *Drosophila* but also in the mammalian system. In fact, the amino acid sequences harbouring the respective Serine residue in the CSL beta-trefoil domain are completely conserved between vertebrates and invertebrates (Wilson and Kovall, 2006; Nagel et al., 2017), raising the possibility of a likewise regulatory mechanism in mammalian hematopoiesis and immunity. Indeed, respective phosphorylation of the human CSL protein at the homologous position S195 was observed in human embryonic stem cells, where differentiation was induced by phorbol ester treatment (Rigbolt et al., 2011), consistent with an involvement of PKCs in this context as well. In conclusion, our work uncovers an important role for PKC-mediated downregulation of CSL activity, thereby ensuring blood cell homeostasis and an appropriate immune response to parasitoid wasp infestation in *Drosophila*. Future work may uncover, whether similar mechanisms apply to mammalian hematopoiesis and immunity as well.

483 **Materials and Methods**

484 **Key resources are listed in S1 Table**

485

486 ***Maintenance of parasitoid wasps and infection assay of Drosophila melanogaster***

487 *Leptopilina boulardi* (*L. boulardi*), *Leptopilina heterotoma* (*L. heterotoma*) and *Asobara*
488 *japonica* (*A. japonica*) were kindly provided by B. Häußling and J. Stökl, Bayreuth, Germany
489 (Weiss et al., 2015). Wasp species were co-cultured with wild-type *Drosophila* larvae at room
490 temperature. To this end, about forty 3-5 days old female wasps and twenty male wasps were
491 co-incubated with second instar larvae for 5-7 days at room temperature. Every other day, fresh
492 drops of honey water were added to the vial plug for feeding the wasps. After two weeks, all
493 hatched flies were discarded. Wasps emerge about 30 days after the infestation.
494 For the infection assays, 50-100 staged *Drosophila* late second/early third instar larvae of the
495 respective genotype were transferred onto apple juice plates with fresh yeast paste. 30 female
496 and 20 male wasps aged between 3-6 days were added to the larvae, allowing to infect them for
497 4-6 hours. Afterwards, wasps were removed and larvae were allowed to develop further in vials
498 with normal fly food. Wasps were only used once for each infection. Only infected larvae
499 containing wasp egg were used for the subsequent experiments. After infestation, hemolymph
500 or lymph glands were prepared at the time points indicated for the particular application, or the
501 survival rate of wasps versus *Drosophila* imago was recorded.

502

503 ***Fly work and genetic analyses***

504 Fly crosses were performed with 30-40 virgin females and 20 males to avoid overcrowding and
505 stress. Combination/recombination of fly stocks was monitored by PCR-genotyping using
506 primers listed in S2 Table. A complete list of the Kinase mutant flies tested in the 'larval kinase
507 screen' is found in Figure 3 – supplement Table 3. As reporter lines served *atilla*-GFP
508 (BL23540) and *PPO3*-Gal4 UAS mCD8-GFP (named *PPO3::GFP*, Dudzic et al., 2015), *hml*Δ-
509 Gal4 UAS-GFP (named *hml::GFP* herein, BL30142) (Sinenko *et al.* 2004) and *He*-Gal4 UAS-
510 GFP (BL8700) (Zetterval *et al.,* 2004). For Gal4/UAS based overexpression and RNAi-
511 mediated knockdown, we used *hml*-Gal4 (BL30141), *lz*-Gal4 (Lebestky *et al.*, 2000; obtained
512 from M. Crozatier, Université de Toulouse, France), UAS-*μMCas9* (VDRC 340002), UAS-
513 HA-*Pkc53E* (this study), UAS-*white-RNAi* (BL31231), UAS-*Pkc53E*-RNAi^{27491} (BL27491),
514 UAS-*Pkc53E*-RNAi^{34716} (BL34716), UAS-*sgRNA-Pkc53E* (VDRC341127) and UAS-*N-RNAi*
515 (BL7078). The strain *vasa-φC31*, *96E-attB*/TM3 (Bischof *et al.*, 2007) served for the
516 generation of UAS-HA-Pkc53E flies. Su(H) controls and mutants comprised: *Su(H)^{gwt}*,

517 *Su(H)*$^{gwt\text{-}mCh}$, *Su(H)*^{S269A} and *Su(H)*^{S269D}/*CyO-GFP*, (Praxenthaler *et al.*, 2017; Frankenreiter et
518 al., 2021). *Su(H)*$^{S269A\text{-}mCh}$ flies were produced in this study by a C-terminal in frame fusion of
519 mCherry to the *Su(H)*^{S269A} mutant gene followed by genomic integration of the construct via
520 gene engineering as outlined before (Praxenthaler *et al.*, 2017).
521
522 ***Generation of the UAS-HA-Pkc53E fly line***
523 *Pkc53E* cDNA (DGRC GH03188) was PCR amplified and subcloned via *Xho*I/*Xba*I in a
524 modified pBT-HA vector, harbouring three copies of an HA-Tag generated via annealed oligos
525 cloned into *Acc*65I/*Xho*I to generate pBT-3xHA-*Pkc53E*. HA-*Pkc53E* was then shuttled via
526 *Acc*65I/*Xba*I in likewise opened pUAST-attB vector (Bischof et al., 2007). All cloning steps
527 were sequence verified. Primers used for cloning are included in S2 Table. Transgenic fly lines
528 were then generated with the help of the φC31 integrase-based system using 96E as landing site
529 (Bischof et al., 2007).
530
531
532 **<u>Analyses of *Drosophila* hematopoetic cells and tissues</u>**
533 ***Recording total hemocyte numbers***
534 Hemocytes were visualized by GFP fluorescence. To this end, *Su(H)*^{gwt}, *Su(H)*^{S269A} and
535 *Pkc53E*$^{\Delta 28}$ alleles, respectively, were combined with *hml*-Gal4 UAS-GFP (BL30142) and *He*-
536 Gal4 UAS-GFP (BL8700) that together label the vast majority of hemocytes (Petraki, *et al.*,
537 2015). Larvae were vortexed at maximum speed with glass beads for 2 min, and the hemolymph
538 was collected individually in 20 µl PBS. A fourth of the hemolymph was distributed in six Pap-
539 pen wells of about 2 mm diameter. To ease staging and to avoid overcrowding, 4 h egg
540 collections were used, and larvae developed in batches of about 100 animals at 25ºC until
541 wandering third instar larval stage (ca. 120 h after egg laying (AEL)). In case of wasp challenge,
542 staged early L3 larvae were infested (ca. 90 h AEL) and bled 20-32 h thereafter to determine
543 total hemocyte numbers. Only larvae containing wasp eggs were examined. GFP-positive
544 hemocytes were visualized by epi-fluorescence microscopy on an Axioskop II (Zeiss, Jena),
545 pictured with an EOS 700D camera (Canon, Japan). For counting cells, we followed earlier
546 descriptions (Petraki *et al.,* 2015). For reproducibility, the 'trainable Weka segmentation'
547 plugin was used to demarcate cells from background (Eibe *et al.*, 2016), followed by the
548 'analyse particles' plugin of Image J. Each Pap-pen well count was taken as a technical replicate
549 for the individual larvae to determine the average hemocyte number per µl, expanded by 20 for
550 the total hemocyte number per larva.

551 ***Determination of sessile larval crystal cells***

552 Larval crystal cells were counted according to Frankenreiter *et al.*, 2021. Briefly, staged
553 wandering third instar larvae of the respective genotype were heated to 60°C for 10-12 min.
554 Pictures of the posterior dorsal side were taken with a Pixera camera (ES120, Optronics, Goleta,
555 USA) mounted to a stereo-microscope (Wild M3Z, Leica, Wetzlar, Germany) with Pixera
556 Viewfinder 2.5. Melanized crystal cells appear as black dots, and were counted in the last two
557 larval segments with *ImageJ* 1.51 software using *Cell Counter* tool. At least twenty larvae were
558 scored for the statistical evaluation. For the PMA/STAU-feeding experiments, 20-30
559 developmentally synchronized second instar larvae were selected and grown for 24 h in
560 complete dark at 25ºC on fly food with 200 µl of 1 mM Phorbol-12-myristat-13-acetat (PMA)
561 or PMA plus 0.2 mM Staurosporine (STAU) added to the surface of the fly food. As PMA and
562 STAU were dissolved in DMSO before further dilution, controls were exposed accordingly to
563 10% DMSO on the fly food. Subsequently, wandering third instar larvae were heated and
564 analysed as above.

565 ***Visualization and quantification of lamellocytes***

566 The lamellocyte specific reporters *atilla*-GFP or *PPO3*::GFP strains were re/combined with
567 $Su(H)^{gwt}$, $Su(H)^{S269A}$ or $Pkc53E^{\Delta 28}$ alleles by genetic means. Late second/early third larval
568 instars were infested by *L. boulardi* and the number of lamellocytes was determined two days
569 later and compared with those observed in non-infested larvae. Larvae were washed thoroughly
570 in cold PBS and dried with a tissue and teared apart. The hemolymph of 10 larvae each was
571 collected with a 20 µl Microloader tip (Eppendorf, Hamburg, Germany) and placed on a slide
572 with 7 µl of Vectashield mounting medium containing DAPI. GFP-positive cells, i.e.
573 lamellocytes were counted in relation to the total number of DAPI labelled hemocytes with a
574 Zeiss Axioskop II and a PlanNeofluar 20x objective. 8-10 independent bleedings were
575 performed each.

576 ***Pkc53E expression in hemocytes***

577 *Pkc53E-eGFP* flies are derived from a protein trap and express endogenously a respective
578 fusion protein (Lee *et al.,* 2018). The hemolymph of three to five third instar *Pkc53E-eGFP*
579 larvae at around 100 h AEL, non-infested or infested at 80 h AEL overnight with *L. boulardi*,
580 was collected as described above in 20 µl cold PBS. Hemocytes were allowed to settle for 5-10
581 min in 500 µl cold PBS onto a round 18 mm glass slide placed in a 12-well microtiter plate.
582 After fixation in 1ml 4% paraformaldehyde in PBS for 15 min at room temperature, three
583 washes with PBS plus 0.3% TritonX100 (PBX), and a pre-incubation step in 500µl 4% normal
584 donkey serum in PBX for 45 min, cells were incubated over night at 4ºC with primary

585 antibodies in 4% donkey serum in PBX (anti-GFP 1:100; anti-He 1:50; anti-Hnt 1:20, anti-mys
586 1:10, anti-PPO1 1:3; anti-Pzg 1:500, rhodamine-coupled phalloidin (1:200-1:400). Depending
587 on the combination, staining with Wheat Germ Agglutinin (WGA, 1:200) was performed for
588 15 min (hnt) and 60 min (PPO1) at room temperature. Three further washing steps and a pre-
589 incubation step as above were followed by incubation for two hours at room temperature with
590 suitable secondary antibodies (1:200) in the dark, followed by three additional washing steps.
591 Cells were mounted in Vectashield by placing the round coverslip upside down on a glass slide,
592 and pictures taken with a BioRad MRC1024 coupled to Zeiss Axioskop with a PlanNeofluar
593 63x objective using LaserSharp software 2000 (Zeiss, Jena, Germany).

594 ***Immunostaining and documentation of larval lymph glands***

595 Larval lymph glands were prepared 24-36 h after wasp infection and treated as described before
596 (Frankenreiter *et al.*, 2021). For comparison, non-infested lymph glands were prepared. Primary
597 antibodies used for staining: mouse anti-Hnt for crystal cells (1:20) and guinea pig anti-Pzg as
598 nuclear marker (1:500). GFP signals were monitored directly. Secondary fluorescent antibodies
599 were from Jackson Immuno-Research Laboratories (1:250 each). Mounted tissue was
600 documented with a Zeiss Axioskop coupled with a BioRad MRC1024 confocal microscope
601 using LaserSharp software 2000 (Zeiss, Jena, Germany). For statistical evaluation at least 12
602 primary lobes were documented and statistically analysed by using *Image J* software
603 (Schindelin et al., 2012). Indices represent the number of cells in relation to the size/area of the
604 tissue (in pixel) x 10000.

605

606 **<u>RNA expression analyses</u>**

607 ***RT-PCR of Pkc53E$^{\Delta 28}$ null mutants and in hemocytes***

608 Poly(A)$^+$ RNA was isolated from 50 third instar larvae (*Pkc53E$^{\Delta 28}$* and *y^{1}w^{67c23}*) using
609 PolyATract System Kit 1000 according to the manufacturer's protocol, followed by a 10 min
610 DNase I treatment at 37°C. Subsequent cDNA synthesis was conducted with qScriber cDNA
611 Synthesis Kit according to the supplier's protocol. For amplification, a *Pkc53E* primer pair
612 overlapping the last three introns was chosen (Pkc53E_RT-PCR UP and Pkc53E_RT-PCR LP).
613 Tubulin 56D primers (Tub56D_229 UP and Tub56D_507 LP) served as internal controls. For
614 primers, see S2 Table. In order to monitor *Pkc53E* expression in hemocytes, hemolymph was
615 derived from 20 third instar *Su(H)^{gwt}* larvae, and poly(A)$^+$ RNA isolated using the Dynabeads
616 micro mRNA-Kit, with an on-beads DNase I digest, otherwise following the above protocol
617 with primer pair Pkc53E_RT-PCR UP and Pkc53E_RT-PCR LP.

618 ***Quantification of NRE-GFP transcription in hemocytes***

619 *Su(H)*^{gwt} or *Su(H)*^{S269A} stocks were genetically combined with NRE-GFP (BL30728).
620 Hemolymph was collected from 15-30 early third instar larvae of each genotype, infested with
621 *L. boulardi* for 6 h at 72h AEL as described above, to be compared with non-infested *Su(H)*^{gwt}
622 control. Poly(A^+) RNA was isolated directly thereafter (0-6 h value) or 24 h later (24-30 h
623 value) with Dynabeads mRNA (micro) Kit from the cells lysed in 200 µl lysis and binding
624 buffer according to the manufacturer's protocol, followed by an on beads DNase I digest for 10
625 min at 37°C. After two washing steps, mRNA was eluted with 25 µl 10 mM Tris-HCl pH8.
626 cDNA synthesis was conducted with 15 µl using the qScriber cDNA Synthesis Kit according
627 to the supplier's protocol. Real-time qPCR was performed as described before using the Blue
628 S'Green qPCR Kit and the MIC magnetic induction cycler (bms, Australia), including target
629 and no-template controls (Kober et al., 2019). Four biological replicates with two technical
630 replicates were each conducted. Results were compared to the ubiquitously expressed genes
631 *cyp33* and *Tbp* as reference. Primer pairs are listed in S2 table. The micPCR® software version
632 2.12.7 was used for relative quantification of the data, based on REST and taking target
633 efficiency into account (Pfaffl et al., 2002).
634
635
636 **Determination of kinases and kinase assays**
637 ***Screening of protein kinase candidates in silico and in vitro***
638 To search for potential candidates in silico, GPS3.0 software was used at the lowest threshold
639 levels, including the 40 kinases with the highest difference between score and cut-off value
640 (Xue *et al.*, 2011). The corresponding *Drosophila* kinases were determined with the help of
641 flybase according to (Morrison et al., 2000). For the *in vitro* screen, a 0.5kb cDNA fragment
642 (741-1242) encoding the Su(H) beta-trefoil domain (codons 247-414), was PCR-amplified and
643 cloned via *Bam*HI/ *Eco*RI into pGEX-2T vector (Smith and Johnson, 1988) for bacterial
644 expression and purification of the BTD-GST fusion protein. Primers used for cloning are
645 included in S2 Table. ProQinase GmbH (Freiburg, Germany) provided the 'KinaseFinder assay
646 service'. Briefly, BTD-GST and ^{33}P-ATP served as substrates for 245 human Ser/Thr kinases
647 in multi-well plates, analysed in a microplate scintillation reader. (A) Activity of each kinase
648 was determined, (B) corrected for substrate background activity, and (C) auto-phosphorylation
649 (kinase activity without substrate). A ratio value between phosphorylation of BTD-Su(H) and
650 kinase auto-phosphorylation ≥1 (A-B/C) was considered as phosphorylating.
651 ***In vitro ADP-Glo^{TM} kinase assay***

652 *Drosophila* pBT-3xHA-*Pkc53E* was mutated to generate the pseudo-activated form
653 *Pkc53E*^{EDDD} (A34E/T508D/T650D/S669D) stepwise by site directed mutagenesis using the
654 Q5® Site directed Mutagenesis Kit. Primers used for mutagenesis are included in S2 Table.
655 *Pkc53E* as well as *PKC53E*^{EDDD} were then shuttled into a modified pMAL vector (Riggs, 1994)
656 where additional restriction sites for *Acc*65I, *Sac*II and *Xho*I had been included in the multiple
657 cloning site via primer annealing. The MBP-Pkc53E and MBP-Pkc53E^{EDDD} fusion proteins
658 were bacterially expressed and purified with Amylose resin. Additionally, activated human
659 kinase PKCα was obtained as a positive control. The PKCα pseudo-substrate PS
660 (RFARLG**S**LRQKNV) (Kochs et al., 1993), the wild type Su(H) peptide S^{wt}
661 (ALFNRLR**S**QTVSTRY) and the phospho-deficient peptide S^{SA} (ALFNRLR**A**QTVSTRY)
662 were obtained (peptides & elephants, Henningsdorf, Germany).
663 To test kinase activity, the ADP-Glo™ Kinase Assay system was used. Kinase assay reactions
664 were performed in 96 well plates in a volume of 25 µl in the dark. Each reaction contained 100
665 µM of a kinase substrate peptide, 150 ng purified kinase and 500 µM ultra-pure ATP. To
666 stimulate kinase activity, 150 nM Phorbol 12-myristate 13-acetate (PMA) was added to some
667 reactions. The mixture was filled up with Kinase reaction buffer (40 mM Tris-HCl, 20 mM
668 $MgCl_2$, 0.1 mg/ml BSA, pH 7.4) and incubated at room temperature for 1 h in the dark. 25 µl
669 ADP-Glo Reagent were added and incubated for 40 min to remove residual ATP. 50 µl of
670 Kinase Detection Reagent was applied to convert ADP to ATP. The luminescent signal was
671 measured after 45 min using GloMax® Discover Microplate Reader (Promega, Madison, USA),
672 kindly provided by the Department of Zoology (190z), University of Hohenheim.
673 ***NanoLC-ESI-MS/MS analysis of Su(H) peptides***
674 Nano-LC-ESI-MS/MS experiments were performed by the Mass Spectrometry Unit at the Core
675 Facility Hohenheim (640) on an Ultimate 2000 RSLCnano system coupled to a Nanospray Flex
676 Ion Source and a Q-Exactive HF-X mass spectrometer (Thermo Fisher Scientific, Waltham,
677 USA). Peptides were separated with LTQ-Orbitrap XL coupled to a nano-HPLC operated under
678 the control of XCalibur 4.1.31.9 software (Thermo Fisher Scientific, Waltham, USA). For all
679 measurements using the Orbitrap detector, internal calibration was as described before (Olsen
680 et al., 2005). MS/MS spectra were analysed using Proteome Discoverer 2.2 (ThermoFisher
681 Scientific, Waltham, United States), verified by manual inspection of the MS/MS spectra
682 (Voolstra et al., 2010).
683
684 ***Generation of a α-pS269 antiserum***

685 Rabbit polyclonal p-S269 Su(H) antiserum was generated by DAVIDS Biotechnology GmbH
686 (Regensburg, Germany) using the synthetic phospho-peptide NRLR**pS**QTVSTRYLHVE.
687 Phospho-specific antibodies were enriched in a depletion-step by affinity purification against
688 the non-phosphorylated peptide. We note a very low affinity of the purified antiserum for Su(H)
689 protein. The antiserum detects purified Su(H)-GST fusion proteins (wild type, S269A as well
690 as S269D) with low affinity in Western blots, but neither native Su(H) in tissue nor hemocytes
691 nor in Western blots, except if phosphorylated and enriched by Trap-technology.
692
693 ***Immunoprecipitation of mCherry and Myc-tagged Su(H)***
694 400 adult heads or 25 larvae of each genotype were homogenized on ice in 220 µl buffer 1 (150
695 mM NaCl, 1% Triton X-100, 50 mM Tris-HCl pH 7.5, 0.1% SDS, supplemented with protease
696 inhibitor cocktail) and incubated for 15 min. After a short spin, 20 µl of the supernatant was set
697 aside as input fraction ('protein extract'). The residual supernatant was diluted with 300 µl wash
698 buffer I (see buffer I, but without Triton X-100). 15 µl of equilibrated magnetic RFP-Trap
699 Magnetic Agarose beads were added, incubated for 1 h at 8°C and washed three times with
700 wash buffer I. mCherry-trapped proteins were resolved on SDS-PAGE; Western blots were
701 probed with rabbit anti-mCherry (1:1000) and rat anti-HA (1:500). Goat secondary antibodies
702 coupled with alkaline phosphatase (1:1000) were used for detection.
703
704 **<u>HeLa cell culture experiments and Luciferase assays</u>**
705 ***Generation of HSV-TK 2xMyc-Su(H)-VP16***
706 Two myc-tags were added to *Su(H)* cDNA in pBT (Maier et al., 2011) by insertion of the two
707 annealed oligonucleotides Myc-Tag UP and Myc-tag LP into the *Eco*RI site (for primers, see
708 S2 Table). The construct was subsequently shuttled via *Eco*RI/*Xho*I into pCDNA3.1. A VP16
709 activator domain was then cloned in frame at the C-terminus of 2xMyc-*Su(H)* by replacing the
710 829 bp *BspE*I/*Apa*I fragment of pCDNA3 2xMyc-*Su(H)* with a respective1060 bp fragment of
711 the pUAST *Su(H)-VP16* construct (Cooper et al., 2000). Then the CMV Promoter of pCDNA3
712 2xMyc-Su(H)-VP16 was replaced by the HSV-TK Promoter of the pRL TK Vector. To this
713 end, the 1023 bp *Bgl*II/*Nhe*I fragment from pRL TK was cloned into the *Bgl*II/*Spe*I opened
714 pCDNA3 *2xMyc- Su(H)*^{VP16} construct.
715 ***Transfection of HeLa cells and reporter assay***
716 *RBPj*^{KO} HeLa cells were cultivated and transfected as described (Wolf et al., 2019). The
717 following constructs were used: pGL3 NRE-reporter (Bray et al., 2005), pCDNA3 HSV-TK
718 2xMyc Su(H)^{VP16} and pRL TK. For the Luciferase assay, 1 x 10^5 HeLa *RBPj*^{KO} cells were

719 seeded in each well of a 12-well cell culture plate. After 24 h the cells were transfected with
720 500 ng pGL3 NRE-reporter, 460 ng pCDNA3 HSV-TK 2xMyc Su(H)^{VP16} and 40 ng pRL-TK.
721 4 h after the transfection the cells were treated with 162 nM PMA, 162 nM PMA plus 21.4 nM
722 Staurosporine (STAU) or 21.4 nM STAU alone. Control cells were treated with the same
723 volume of DMSO present in the other treatments. 14 hours later, cells were washed twice in
724 PBS pH 7.4 and lysed in 75 µl 1x Passive Lysis Buffer. The Dual-Luciferase® Reporter Assay
725 was performed according to the manufacturer's instructions.
726 Su(H)-VP16 expression levels were detected with anti-Myc mAB (1:500) and anti beta-tubulin
727 as loading control (1:500). To this end, 5 x 10^5 HeLa *RBPj^{KO}* cells were transfected and treated
728 as above, harvested and lysed 14 h later in 300 µl binding buffer (20 mM HEPES pH 7.6, 150
729 mM $MgCl_2$, 10% glycerol, 0.05% NP-40, 1 mM DTT, ROCHE cOmplete™ ULTRA-tablet
730 Mini protease inhibitor); 20 µl of each lysate were loaded for Western blotting.
731
732 ***Statistical analysis and documentation of data***
733 Normality of the data was checked by a Shapiro-Wilk test using GraphPad Prism 9.0. In case
734 of normally distributed data, a two-tailed analysis of variance (ANOVA) approach for multiple
735 comparisons according to Tukey-Kramer's Honestly Significance Difference or an unpaired t-
736 test was applied, and in the other cases the non-parametric Kruskal-Wallis sum test or Dunn's
737 test for multiple comparisons. Quantification of RT-PCR data is based on REST, and was
738 performed with the micPCR® software version 2.12.7, taking target efficiency into account
739 (Pfaffl et al., 2002). In the figures, p-values are presented as ***, $p<0.001$; **, $p<0.01$; *,
740 $p<0.05$; not significant, $p\geq0.5$; the exact p-values are given in the respective source data.
741 Pictures were assembled using ImageJ, PhotoPaint, CorelDraw and BoxPlotR software. In the
742 box plots made by BoxPlotR, center lines show the medians; box limits indicate the 25th and
743 75th percentiles as determined by R software; whiskers extend 1.5 times the interquartile range
744 from the 25th and 75th percentiles, outliers are represented by dots. Number of sample points
745 is given in the figure or legend.

746 **Data availability**

747 All data are contained within the manuscript.

748

749 **Acknowledgments**

750 We are deeply grateful to Benedikt Häußling and Johannes Stökl (University of Bayreuth,
751 Germany) for sending us all wasp species used in this study and for giving SD and LF a basic
752 course in handling of the wasps. We thank Michèle Crozatier (Toulouse, France), David
753 Hipfner (Montréal, Canada), Bruno Lemaitre (Lausanne, Switzerland), Sarah Bray (Cambridge,
754 UK), Dieter Maier (Hohenheim, Germany), the Bloomington *Drosophila* Stock Center (BDSC,
755 NIH P40OD018537) and the Vienna *Drosophila* Stock Center (VDRC) for numerous fly
756 stocks. We acknowledge the Drosophila Genomics Resource Center (DGRC, NIH
757 2P40OD010949) for sending the Pkc53E cDNA, and the Developmental Studies Hybridoma
758 Bank (DSHB), created by the NICHD of the NIH and maintained at the University of Iowa,
759 Department of Biology, Iowa City, IA 52242 for providing several monoclonal antibodies. We
760 thank Istvan Andó (Szeged, Hungary) for anti-Hemese antiserum, and Tina E. Trenczek
761 (Gießen, Germany) for anti-PPO1 antibodies. We very much acknowledge Franz Oswald (Ulm,
762 Germany) and Tilman Borggrefe (Gießen, Germany) for the $RBPj^{KO}$ HeLa cell line. We are
763 indebted to Lisa Lermer for her help in tissue preparations and screening of larvae and Janika
764 Scharpf for the purification of the Pkc53E proteins. We are grateful to Armin Huber,
765 Department of Biochemistry, for the use of the Apotome microscope, to Axel Schweickert,
766 Department of Zoology, for use of the GloMax® Discover Microplate Reader and to Jens
767 Pfannstiel at the Mass Spectrometry Unit (Core Facility of the University of Hohenheim) for
768 the MS/MS and ESI spectra. We thank Dieter Maier for helpful comments on the manuscript.

769 **References**

770 Altman, A., Kong, K.F. (2016). Protein Kinase C Enzymes in the Hematopoietic and Immune
771 Systems. *Annu Rev Immunol*. 34:511-538. doi:10.1146/annurev-immunol-041015-055347
772 Anderl, I., Vesala, L., Ihalainen, T. O., Vanha-Aho, L. M., Andó, I., Rämet, M., Hultmark, D.
773 (2016). Transdifferentiation and Proliferation in Two Distinct Hemocyte Lineages in
774 *Drosophila melanogaster* Larvae after Wasp Infection. *PLoS Pathog*. 12(7):e1005746.
775 doi:10.1371/journal.ppat.1005746
776 Banerjee, U., Girard, J.R., Goins, L.M., Spratford, C.M. (2019). *Drosophila* as a genetic
777 model for hematopoiesis. *Genetics* 211(2):367-417. doi:10.1534/genetics.118.300223.
778 Bischof, J., Maeda, R.K., Hediger, M., Karch, F., Basler, K. (2007). An optimized
779 transgenesis system for *Drosophila* using germ-line-specific phiC31 integrases. Proc Natl
780 Acad Sci USA 104(9):3312-3317. doi:10.1073/pnas.0611511104
781 Blanco-Obregon, D., Katz, M.J., Durrieu, L., Gándara, L., Wappner, P. (2020). Context-
782 specific functions of Notch in *Drosophila* blood cells progenitors. *Dev Biol* 462(1):101-
783 115. doi:10.1016/j.ydbio.2020.03.018
784 Blumberg, P.M., Delclos, K.B., Dunn, J.A., Jaken, S., Leach, K.L., Yeh, E. (1983). Phorbol
785 ester receptors and the in vitro effects of tumor promoters. *Ann N Y Acad Sci*. 407:303-315.
786 doi:10.1111/j.1749-6632.1983.tb47836.x
787 Borggrefe, T., Oswald, F. (2009). The Notch signaling pathway: transcriptional regulation at
788 Notch target genes. *Cell Mol Life Sci*. 66(10):1631-1646. doi:10.1007/s00018-009-8668-7
789 Bray, S.J. (2016). Notch signalling in context. *Nat Rev Mol Cell Biol*. 17(11):722-735.
790 doi:10.1038/nrm.2016.94
791 Bray, S., Musisi, H., Bienz, M. (2005). Bre1 is required for Notch signaling and histone
792 modification. *Dev Cell* 8(2):279-286. doi: 10.1016/j.devcel.2004.11.020
793 Cattenoz, P. B., Sakr, R., Pavlidaki, A., Delaporte, C., Riba, A., Molina, N., Hariharan, N.,
794 Mukherjee, T., Giangrande, A. (2020). Temporal specificity and heterogeneity of
795 *Drosophila* immune cells. *EMBO J*. 39(12):e104486. doi:10.15252/embj.2020104486
796 Chakrabarti, S., Visweswariah, S.S. (2020). Intramacrophage ROS Primes the Innate Immune
797 System via JAK/STAT and Toll Activation. *Cell Rep*. 33(6):108368.
798 doi:10.1016/j.celrep.2020.108368
799 Cherbas, L., Willingham, A., Zhang, D., Yang, L., Zou, Y., Eads, B.D., Carlson, J.W.,
800 Landolin, J.M., Kapranov, P., Dumais, J., *et al*. (2011). The transcriptional diversity of 25
801 *Drosophila* cell lines. *Genome Res*. 21(2):301-314. doi:10.1101/gr.112961.110

802 Cho, B., Yoon, S. H., Lee, D., Koranteng, F., Tattikota, S. G., Cha, N., Shin, M., Do, H., Hu,
803 Y., Oh, S. Y., *et al.* (2020). Single-cell transcriptome maps of myeloid blood cell lineages
804 in *Drosophila*. *Nat. Commun*. 11:4483. doi:10.1038/s41467-020-18135-y.
805 Cosentino-Gomes, D., Rocco-Machado, N., Meyer-Fernandes, J. R. (2012). Cell signaling
806 through protein kinase C oxidation and activation. *Int J Mol Sci*. 13(9):10697-10721.
807 doi:10.3390/ijms130910697
808 Cooper, M.T., Tyler, D.M., Furriols, M., Chalkiadaki, A., Delidakis, C., Bray, S. (2000).
809 Spatially restricted factors cooperate with Notch in the regulation of Enhancer of split
810 genes. *Dev Biol.*, *221*(2), 390–403. doi:10.1006/dbio.2000.9691
811 Crozatier, M., Ubeda, J.-M., Vincent, A., Meister, M., (2004). Cellular immune response to
812 parasitization in *Drosophila* requires the EBF orthologue collier. *PLoS Biol*. 2:e196.
813 doi:10.1371/journal.pbio.0020196
814 Csordás, G., Gábor, E., Honti, V. (2021). There and back again: The mechanisms of
815 differentiation and transdifferentiation in *Drosophila* blood cells. *Dev Biol*. 469:135-143.
816 doi:10.1016/j.ydbio.2020.10.006
817 Deichsel, S., Gahr, B.M., Mastel, H., Preiss, A., Nagel, A.C. (2024). Numerous
818 Serine/Threonine kinases affect blood cell homeostasis in *Drosophila melanogaster*. *Cells*
819 13(7):576. https://doi.org/10.3390/cells13070576
820 Dudzic, J.P., Kondo, S., Ueda, R., Bergman, C.M., Lemaitre, B. (2015). *Drosophila* innate
821 immunity: regional and functional specialization of prophenoloxidases. *BMC Biol* 13:81.
822 doi: 10.1186/s12915-015-01393-6
823 Duvic, B., Hoffmann, J.A., Meister, M., Royet, J. (2002). Notch signaling controls lineage
824 specification during *Drosophila* larval hematopoiesis. *Curr. Biol*. 12: 1923–1927.
825 doi:10.1016/s0960-9822(02)01297-6
826 Eibe, F., Hall, M.A., Witten, I.H. (2016). The WEKA workbench. Online Appendix for 'Data
827 Mining: Practical machine learning tools and techniques', Morgan Kaufmann, Fourth
828 Edition.
829 Evans, C.J., Liu, T., Girard, J.R., Banerjee, U. (2022). Injury-induced inflammatory signaling
830 and hematopoiesis in *Drosophila*. *Proc Natl Acad Sci U S A*. 119(12):e2119109119.
831 doi:10.1073/pnas.2119109119
832 Ferguson, G.B., Martinez-Agosto, J. A. (2014) Yorkie and Scalloped signaling regulates
833 Notch-dependent lineage specification during *Drosophila* hematopoiesis. *Curr Biol*. 24:
834 2665–2672. doi:10.1016/j.cub.2014.09.081

835 Frankenreiter, L., Gahr, B.M., Schmid, H., Zimmermann, M., Deichsel, S., Hoffmeister, P.,
836 Turkiewicz, A., Borggrefe, T., Oswald, F., Nagel, A.C. (2021). Phospho-site mutations in
837 transcription factor Suppressor of Hairless impact Notch signaling activity during
838 hematopoiesis in *Drosophila*. *Front Cell Dev Biol*. 9:658820.
839 doi:10.3389/fcell.2021.658820
840 Gallenstein, N., Tichy, L., Weigand, M.A., Schenz, J. (2023). Notch Signaling in Acute
841 Inflammation and Sepsis. *Int J Mol Sci*. 24(4):3458. doi:10.3390/ijms24043458
842 Giaimo B.D., Gagliani E.K., Kovall R.A., Borggrefe T. (2021). Transcription Factor RBPJ as
843 a Molecular Switch in Regulating the Notch Response. *Adv Exp Med Biol*. 1287:9-30.
844 doi:10.1007/978-3-030-55031-8_2
845 Ghosh, S., Singh, A., Mandal, S., Mandal, L. (2015). Active hematopoietic hubs in
846 *Drosophila* adults generate hemocytes and contribute to immune response. *Dev. Cell*
847 33:478-488. doi: org/10.1016/j.devcel.2015.03.014
848 Gould C.M., Newton A.C. (2008). The life and death of protein kinase C. *Curr Drug Targets*
849 9(8):614-625. doi:10.2174/138945008785132411
850 Gueguen, G., Kalamarz, M. E., Ramroop, J., Uribe, J., Govind, S. (2013). Polydnaviral
851 ankyrin proteins aid parasitic wasp survival by coordinate and selective inhibition of
852 hematopoietic and immune NF-kappa B signaling in insect hosts. *PLoS Pathog*.
853 9(8):e1003580. doi:10.1371/journal.ppat.1003580
854 Ha, E.M., Lee, K.A., Park, S.H., Kim, S.H., Nam, H.J., Lee, H.Y., Kang, D., Lee, W.J.
855 (2009). Regulation of DUOX by the Galphaq-phospholipase Cbeta-Ca2+ pathway in
856 *Drosophila* gut immunity. *Dev Cell*. 16(3):386-397. doi:10.1016/j.devcel.2008.12.015
857 Honti, V., Kurucz, E., Csordás, G., Laurinyecz, B., Márkus, R., Andó, I. (2009). In vivo
858 detection of lamellocytes in *Drosophila melanogaster*. *Immunol Lett.* 126(1-2):83-84. doi:
859 10.1016/j.imlet.2009.08.004
860 Honti, V., Csordás, G., Márkus, R., Kurucz, E., Jankovics, F., Andó, I. (2010). Cell lineage
861 tracing reveals the plasticity of the hemocyte lineages and of the hematopoietic
862 compartments in *Drosophila melanogaster*. *Mol Immunol*. 47(11-12):1997-2004.
863 doi:10.1016/j.molimm.2010.04.017
864 Hultmark, D., Andó, I. (2022) Hematopoietic plasticity mapped in *Drosophila* and other
865 insects. *eLife* 11:e78906. doi:10.7554/eLife.78906
866 Karaman, M.W., Herrgard, S., Treiber, D.K., Gallant, P., Atteridge C.E., Campbell, B.T.,
867 Chan, K.W., Ciceri, P., Davis, M.I., Edeen, P.T., *et al.* (2008). A quantitative analysis of
868 kinase inhibitor selectivity. *Nat Biotechnol.* 26:127-132. doi: 10.1038/nbt1358.

Kharrat, B., Csordás, G., Honti, V. (2022). Peeling Back the Layers of Lymph Gland Structure and Regulation. *Int J Mol Sci*. 23(14):7767. doi:10.3390/ijms23147767

Kim, S.H., Lee, W.J. (2014). Role of DUOX in gut inflammation: lessons from *Drosophila* model of gut-microbiota interactions. *Front Cell Infect Microbiol*. 3:116. doi:10.3389/fcimb.2013.00116

Kim-Jo C, Gatti J.L., Poirié M. (2019) *Drosophila* Cellular Immunity Against Parasitoid Wasps: A Complex and Time-Dependent Process. *Front Physiol*. 10:603. doi:10.3389/fphys.2019.00603

Kober, L., Zimmermann, M., Kurz, M., Bayer, M., Nagel, A.C. (2019). Loss of *putzig* in the germline impedes germ cell development by inducing cell death and new niche like microenvironments. *Sci Rep* 9(1):9108. doi:10.1038/s41598-019-45655-5

Kochs, G., Hummel, R., Meyer, D., Hug, H., Marmé, D., Sarre, T.F. (1993). Activation and substrate specificity of the human protein kinase C alpha and zeta isoenzymes. *Eur J Biochem*. 216(2):597-606. doi:10.1111/j.1432-1033.1993.tb18179.x

Kopan R, Ilagan M.X. (2009). The canonical Notch signaling pathway: unfolding the activation mechanism. *Cell* 137(2):216-233. doi:10.1016/j.cell.2009.03.045

Kovall, R.A., Blacklow, S.C. (2010). Mechanistic insights into Notch receptor signaling from structural and biochemical studies. *Curr Top Dev Biol*. 92:31-71. doi:10.1016/S0070-2153(10)92002-4

Krzemien, J., Oyallon, J., Crozatier, M., Vincent, A. (2010). Hematopoietic progenitors and hemocyte lineages in the *Drosophila* lymph gland. *Dev. Biol*. 346, 310–319. doi:10.1016/j.ydbio.2010.08.003

Kugler, S.J., Nagel, A.C. (2007). *Putzig* is required for cell proliferation and regulates Notch activity in *Drosophila*. *Mol Biol Cell* 18(10):3733-3740. doi: 10.1091/mbc.e07-03-0263

Kurucz, E., Zettervall, C. J., Sinka, R., Vilmos, P., Pivarcsi, A., Ekengren, S., Hegedüs, Z., Andó, I., Hultmark, D. (2003). Hemese, a hemocyte-specific transmembrane protein, affects the cellular immune response in *Drosophila*. *Proc Natl Acad Sci U S A*. 100(5):2622-2627. doi:10.1073/pnas.0436940100

Lanot, R., Zachary, D., Holder, F., Meister, M. (2001). Postembryonic hematopoiesis in *Drosophila*. *Dev Biol*. 230, 243–257. doi:10.1006/dbio.2000.0123

Lebestky, T., Chang, T., Hartenstein, V., Banerjee, U. (2000). Specification of *Drosophila* hematopoietic lineage by conserved transcription factors. *Science* 288(5463):146-149. doi:10.1126/science.288.5463.146

902 Lebestky, T., Jung, S.-H., Banerjee, U. (2003). A Serrate-expressing signaling center controls
903 *Drosophila* hematopoiesis. *Genes Dev.* 17(3):348-353. doi: 10.11101/gad.1052803
904 Lee, K.A., Kim, B., Bhin, J., Kim, D.H., You, H., Kim, E. K., Kim, S.H., Ryu, J.H., Hwang,
905 D., Lee, W.J. (2015). Bacterial uracil modulates *Drosophila* DUOX-dependent gut
906 immunity via Hedgehog-induced signaling endosomes. *Cell Host Microbe* 17(2):191-204.
907 doi:10.1016/j.chom.2014.12.012
908 Lee, P.T., Zirin, J., Kanca, O., Lin, W.W., Schulze, K.L., Li-Kroeger, D., Tao, R., Devereaux,
909 C., Hu, Y., Chung, V., *et al.* (2018). A gene-specific T2A-GAL4 library for
910 *Drosophila*. *eLife* 7: e35574. doi:10.7554/eLife.35574
911 Letourneau, M., Lapraz, F., Sharma, A., Vanzo, N., Waltzer, L., Crozatier, M. (2016).
912 *Drosophila* hematopoiesis under normal conditions and in response to immune stress.
913 *FEBS Lett*. 590(22):4034-4051. doi: 10.1002/1873-3468.12327
914 Lim, P.S., Sutton, C.R., Rao, S. (2015). Protein kinase C in the immune system: from
915 signalling to chromatin regulation. *Immunology*. 146(4):508-522. doi:10.1111/imm.12510
916 Louradour, I., Sharma, A., Morin-Poulard, I., Letourneau, M., Vincent, A., Crozatier, M.,
917 Vanzo, N. (2017). Reactive oxygen species-dependent Toll/NF-KB activation in the
918 *Drosophila* hematopoietic niche confers resistance to wasp parasitism. *eLife* 6:e25496.
919 doi:10.7554/eLife.25496.
920 McGonigle, J.E., Leitão, A.B., Ommeslag, S., Smith, S., Day, J.P., Jiggins, F.M. (2017).
921 Parallel and costly changes to cellular immunity underlie the evolution of parasitoid
922 resistance in three *Drosophila* species. *PLoS Pathog. 13*(10): e1006683.
923 doi:10.1371/journal.ppat.1006683
924 Maier, D. (2006). Hairless: the ignored antagonist of the Notch signalling pathway. *Hereditas*
925 143:212-221. doi:10.1111/j.2007.0018-0661.01971.x
926 Maier, D., Kurth, P., Schulz, A., Russell, A., Yuan, Z., Gruber, K., Kovall, R.A., Preiss, A.
927 (2011). Structural and functional analysis of the repressor complex in the Notch signaling
928 pathway of *Drosophila melanogaster*. *Mol Biol Cell*. *22*(17):3242–3252.
929 doi:10.1091/mbc.E11-05-0420.
930 Márkus, R., Laurinyecz, B., Kurucz, E., Honti, V., Bajusz, I., Sipos, B., Somogyi, K.,
931 Kronhamn, J., Hultmark, D., Andó, I. (2009). Sessile hemocytes as a hematopoietic
932 compartment in *Drosophila melanogaster*. *Proc Natl Acad Sci U S A*. 106(12):4805-4809.
933 doi:10.1073/pnas.0801766106
934 Morrison, D.K., Murakami, M.S., Cleghon, V. (2000). Protein kinases and phosphatases in
935 the *Drosophila* genome. *J Cell Biol* 150(2):F57-62. doi:10.1083/jcb.150.2.f57.

936 Mukherjee, T., Kim, W.S., Mandal, L., Banerjee, U. (2011). Interaction between Notch and
937 Hif-alpha in development and survival of *Drosophila* blood cells. *Science* 332(6034):1210-
938 1213. doi:10.1126/science.1199643
939 Nagel, A.C., Auer, J.S., Schulz, A., Pfannstiel, J., Yuan, Z., Collins, C. E., Kovall, R.A.,
940 Preiss, A. (2017). Phosphorylation of Suppressor of Hairless impedes its DNA-binding
941 activity. *Sci Rep*. 7(1):11820. doi:10.1038/s41598-017-11952-0
942 Nakashima, S. (2002). Protein kinase C alpha (PKC alpha): regulation and biological
943 function. *J Biochem*. 132(5):669-675. doi:10.1093/oxfordjournals.jbchem.a003272
944 Nappi, A.J., E. Vass, F. Frey, Y. Carton (1995). Superoxide anion generation in *Drosophila*
945 during melanotic encapsulation of parasites. *Eur J Cell Biol*. 68:450–456.
946 Olsen, J.V., de Godoy, L.M.F., Li, G., Mortensen, P., Pesch, R., Makarov, A., Lange, O.,
947 Horning, S., Mann, M. (2005). Parts per million mass accuracy on an Orbitrap mass
948 spectrometer via lock mass injection into a C-trap. *Mol Cell Proteomics* 4(12):2010-2021.
949 doi: 10.1974/mcp.T500030-MCP200
950 Petraki, S., Alexander, B., Brückner, K. (2015). Assaying blood cell populations of the
951 *Drosophila melanogaster* larva. *J Vis Exp*. 105:52733. doi:10.3791/52733
952 Pfaffl, M.W., Horgan, G.W., Dempfle, L. (2002). Relative expression software tool (REST)
953 for a group-wise comparison and statistical analysis of relative expression results in real-
954 time PCR. *Nucleic Acids Res*. 30:e36. doi:10.1093/nar/30.9.e36
955 Praxenthaler, H., Nagel, A.C., Schulz, A., Zimmermann, M., Meier, M., Schmid, H., Preiss,
956 A., Maier, D. (2017). Hairless-binding deficient Suppressor of Hairless alleles reveal
957 Su(H) protein levels are dependent on complex formation with Hairless. *PLoS Genet*.
958 13(5):e1006774. doi: 10.1371/journal.pgen.1006774
959 Radtke, F., Fasnacht, N., Macdonald, H.R. (2010). Notch signaling in the immune system.
960 *Immunity* 32(1):14-27. doi:10.1016/j.immuni.2010.01.004
961 Razzell, W., Evans, I.R., Martin, P., Wood, W. (2013). Calcium flashes orchestrate the wound
962 inflammatory response through DUOX activation and hydrogen peroxide release. *Curr*
963 *Biol*. 23(5):424-429. doi:10.1016/j.cub.2013.01.058
964 Rigbolt, K.T., Prokhorova, T.A., Akimov, V., Henningsen, J., Johansen, P.T., Kratchmarova,
965 I., Kassem, M., Mann, M., Olsen, J.V., Blagoev, B. (2011). System-wide temporal
966 characterization of the proteome and phosphoproteome of human embryonic stem cell
967 differentiation. *Sci Signal*. 4(164):rs3. doi:10.1126/scisignal.2001570
968 Riggs, P. (1994) Expression and Purification of Maltose-Binding Protein Fusions. *Curr.*
969 *Protoc. Mol. Biol. 28*, 16.6.1-16.6.14. 855 doi:10.1002/0471142727.mb1606s28. 856

970 Rizki, T.M. (1957). Alterations in the haemocyte population of *Drosophila melanogaster*. *J.*
971 *Morphol*. 100, 437–458. doi: 10.1002/jmor.1051000303
972 Sanchez Bosch, P.S., Makhijani, K., Herboso, L., Gold, K.S., Baginsky, R., Woodcock, K.J.,
973 Alexander, B., Kukar, K., Corcoran, S., Jacobs, T., *et al.* (2019). Blood cell reservoir at the
974 respiratory epithelia top relay infection signals to surrounding tissues. *Dev Cell* 51:787-
975 803. doi: 10.1016/j.devcel.2019.10.017
976 Schindelin, J., Arganda-Carreras, I., Frise, E., Kaynig V, Longair M, Pietzsch T, Preibisch, S.,
977 Rueden, C., Saalfeld, S., Schmid, B., *et al.* (2012). Fiji: an open-source platform for
978 biological-image analysis. *Nat Methods* 9:676–682. doi:10.1038/nmeth.2019
979 Schlenke, T.A., Morales, J., Govind, S., Clark, A.G. (2007). Contrasting infection strategies
980 in generalist and specialist wasp parasitoids of *Drosophila melanogaster*. *PLoS Pathog*.
981 3(10):1486-1501. doi:10.1371/journal.ppat.0030158
982 Schneider, I. (1972). Cell lines derived from late embryonic stages of *Drosophila*
983 *melanogaster*. *J Embryol Exp Morphol*. 27:353-365.
984 Shifera, A.S., Hardin, J.A. (2009). PMA induces expression from the herpes simplex virus
985 thymidine kinase promoter via the activation of JNK and ERK in the presence of
986 adenoviral E1A proteins. *Arch Biochem Biophys*. 490(2):145-157.
987 doi:10.1016/j.abb.2009.08.013
988 Siebel C., Lendahl U. (2017). Notch Signaling in Development, Tissue Homeostasis, and
989 Disease. *Physiol Rev*. 97(4):1235-1294. doi:10.1152/physrev.00005.2017
990 Sinenko, S.A., Mathey-Prevot, B. (2004). Increased expression of *Drosophila* tetraspanin,
991 Tsp68C, suppresses the abnormal proliferation of ytr-deficient and Ras/Raf-activated
992 hemocytes. *Oncogene* 23(56):9120-9128. doi:10.1038/sj.onc.1208156
993 Sinenko, S.A., Shim, J., Banerjee, U. (2011). Oxidative stress in the haematopoietic niche
994 regulates the cellular immune response in *Drosophila*. *EMBO Rep*. 13:83–89.
995 doi:10.1038/embor.2011.223
996 Small, C., Ramroop, J., Otazo, M., Huang, L.H., Saleque, S., Govind, S. (2014). An
997 unexpected link between Notch signaling and ROS in restricting the differentiation of
998 hematopoietic progenitors in *Drosophila*. *Genetics* 197(2):471-483. doi:10.1534/genetics
999 Smith, D.B., Johnson, K.S. (1988). Single-step purification of polypeptides expressed in
1000 *Escherichia coli* as fusions with glutathione S-transferase. *Gene* 67(1):31-40.
1001 doi:10.1016/0378-1199(88)90005-4

1002 Sorrentino, R.P., Carton, Y., Govind, S. (2002). Cellular immune response to parasite
1003 infection in the *Drosophila* lymph gland is developmentally regulated. *Dev Biol.*
1004 *243*(1):65–80. doi:10.1006/dbio.2001.0542
1005 Spitzer, M., Wildenhain, J., Rappsilber, J., Tyers, M. (2014). BoxPlotR: a web tool for
1006 generation of box plots. *Nat Methods 11*(2):121–122. doi:10.1038/nmeth.2811
1007 Stofanko, M., Kwon, S.Y., Badenhorst, P. (2010). Lineage tracing of lamellocytes
1008 demonstrates *Drosophila* macrophage plasticity. *PLoS One* 5:e14051.
1009 doi:10.1371/journal.pone.0014051.
1010 Tattikota, S.G., Cho, B., Liu, Y., Hu, Y., Barrera, V., Steinbaugh, M.J., Yoon, S.-H.,
1011 Comjean, A., Li, F., Dervis, F., Hung, R.-J., *et al.* (2020). A single-cell survey of
1012 *Drosophila* blood. *eLife* 9:e54818. doi:10.7554/eLife.54818
1013 Terriente-Felix, A., Li, J., Collins, S., Mulligan, A., Reekie, I., Bernard, F., Krejci, A., Bray,
1014 S. (2013). Notch cooperates with Lozenge/Runx to lock haemocytes into a differentiation
1015 programme. *Development* 140:926–937. doi:10.1242/dev.086785
1016 Trenczek, T., Bennich, H. (1992). Characterization of haemocytes of *Hyalophora cecropia* by
1017 monoclonal antibodies. *Verh Dtsch Zool Ges*. 85:216.
1018 Vanha-Aho, L. M., Anderl, I., Vesala, L., Hultmark, D., Valanne, S., Rämet, M. (2015). Edin
1019 expression in the fat body is required in the defense against parasitic wasps in *Drosophila*
1020 *melanogaster*. *PLoS Pathog*. 11(5):e1004895. doi:10.1371/journal.ppat.1004895
1021 Voolstra, O., Beck, K., Oberegelsbacher, C., Pfannstiel, J., Huber, A. (2010). Light-dependent
1022 phosphorylation of the *Drosophila* transient receptor potential ion channel. *J Biol Chem.*
1023 285, 14275–14284. doi:10.1074/jbc.M110.102053
1024 Weiss, I., Ruther, J., Stökl, J. (2015). Species specificity of the putative male antennal
1025 aphrodisiac pheromone in *Leptopilina heterotoma*, *Leptopilina boulardi* and *Leptopilina*
1026 *victoriae*. *Biomed Res Int*. 2015:202965. doi:10.1155/2015/202965.
1027 Wilson, J.J., Kovall, R.A. (2006). Crystal structure of the CSL-Notch-Mastermind ternary
1028 complex bound to DNA. *Cell* 124(5):985-996. doi:10.1016/j.cell.2006.01.035
1029 Wolf, D., Smylla, T.K., Reichmuth, J., Hoffmeister, P., Kober, L., Zimmermann, M.,
1030 Turkiewicz, A., Borggrefe, T., Nagel, A.C., Oswald, F., *et al.* (2019). Nucleo-cytoplasmic
1031 shuttling of *Drosophila* Hairless/Su(H) heterodimer as a means of regulating Notch
1032 dependent transcription. *Biochim Biophys Acta Mol Cell Res*. 1866(10):1520-1532. doi:
1033 10.1016/j.bbamcr.2019.07.008
1034 Xue, Y., Liu, Z., Cao, J., Ma, Q., Gao, X., Wang, Q., Jin, C., Zhou, Y., Wen, L., Ren, J.
1035 (2011). GPS 2.1: enhanced prediction of kinase-specific phosphorylation sites with an

1036 algorithm of motif length selection. *Protein Eng Des Sel* 24(3):255-260. doi:
1037 10.1093/protein/gzq094
1038 Yashiro-Ohtani, Y., He, Y., Ohtani, T., Jones, M.E., Shestova, O., Xu, L., Fang, T. C.,
1039 Chiang, M.Y., Intlekofer, A.M., Blacklow, S.C., *et al.* (2009). Pre-TCR signaling
1040 inactivates Notch1 transcription by antagonizing E2A. *Genes Dev*. 23(14):1665-1676.
1041 doi:10.1101/gad.1793709.
1042 Yui, M.A., Rothenberg, E.V. (2014). Developmental gene networks: a triathlon on the course
1043 to T cell identity. *Nat Rev Immunol*. 2014;14(8):529-545. doi:10.1038/nri3702
1044 Zettervall, C-J., Anderl, I., Willimas, M.J., Palmer, R., Kurucz, E., Andó, I., Hultmark, D.
1045 (2004). A directed screen for genes involved in *Drosophila* blood cell activation. *Proc Natl*
1046 *Acad Sci USA* 101(39):14192-14197. doi:10.1073/pnas.0403789101.

1047 **Figures**

1048 **Figure 1**

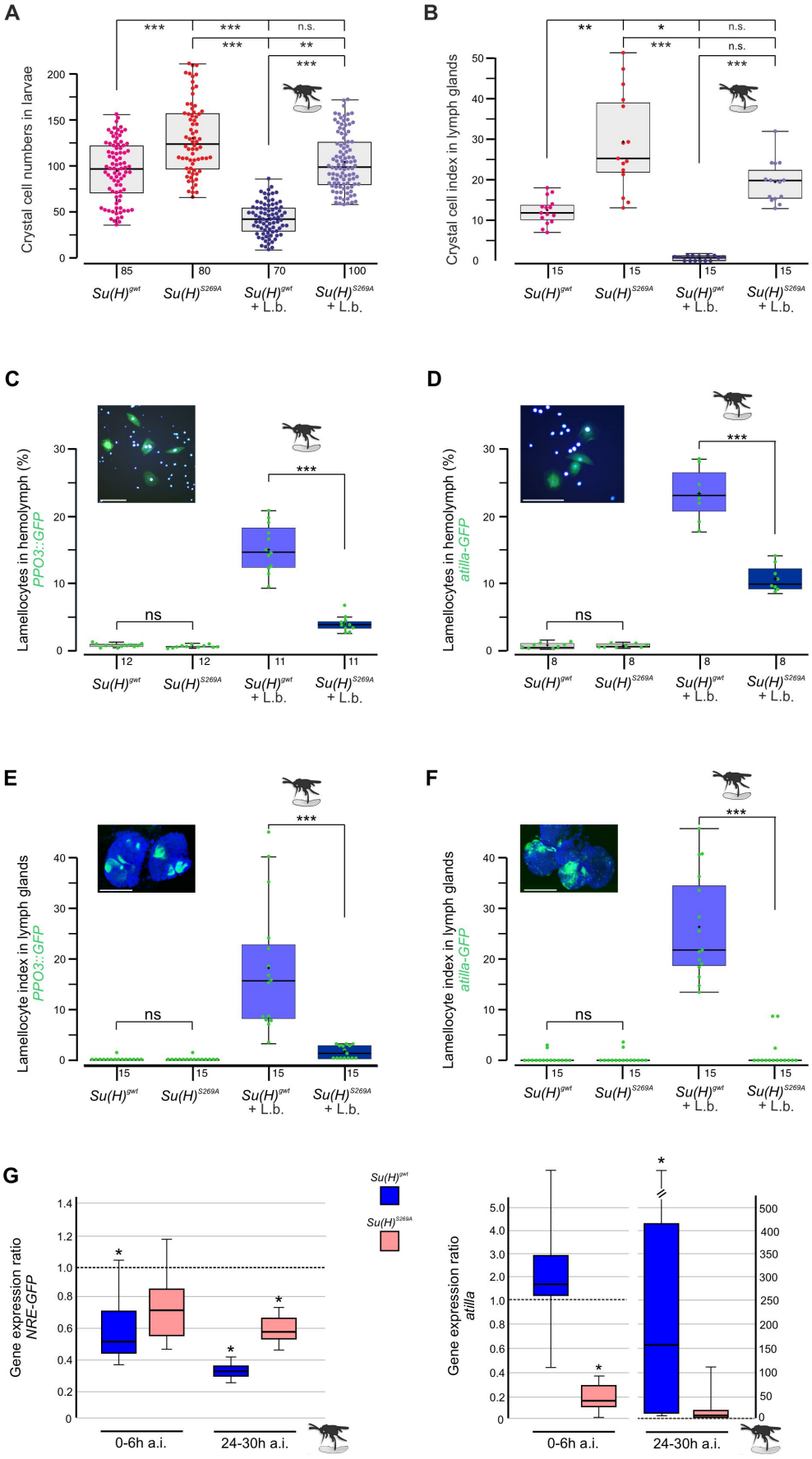

1049

1050

1051 ***Figure 1 Su(H)^{S269A} mutants are compromised in their response to parasitoid wasp***
1052 ***infestation***

1053 (**A**) Quantification of melanized crystal cells from the last two segments of *Su(H)^{gwt}* and
1054 *Su(H)^{S269A}* larvae with and without wasp infestation as indicated. In the control, wasp
1055 parasitism causes crystal cell numbers to drop to a level of about 50%, whereas in *Su(H)^{S269A}*
1056 mutants the number settles at the un-infested *Su(H)^{gwt}* level. Each dot represents one analysed
1057 larva (n=70-100 as indicated). (**B**) Crystal cell index in larval lymph glands is given as ratio
1058 of Hnt-positive crystal cells per 1° lobe relative to the size of the lobe. Each point represents
1059 one analysed lobus (n=15). (A,B) Statistical analyses Kruskal-Wallis test, followed by Dunn's
1060 test with *** $p<0.001$, ** $p<0.01$, * $p<0.05$, ns (not significant $p\geq0.05$).

1061 (**C-F**) Quantification of larval lamellocytes in the circulating hemolymph (C,D) or in lymph
1062 glands (E,F) before and after wasp infestation in *Su(H)^{gwt}* versus *Su(H)^{S269A}*. Lamellocytes
1063 were marked with either *PPO3-Gal4::UAS*-GFP (C,E) or *atilla*-GFP (D,F) as indicated.
1064 (C,D) The fraction of GFP-labelled lamellocytes of the total number of DAPI-labelled blood
1065 cells isolated from hemolymph is given; each dot represents ten pooled larvae (n=8-10 as
1066 shown). Representative image of labelled control hemolymph is shown above (DAPI-labelled
1067 nuclei in light blue, GFP in green). Scale bars 50 µm. (E,F) Lamellocyte index is given as
1068 number of GFP-labelled lamellocytes per area in the 1° lobe of the lymph gland. Each dot
1069 represents the lamellocyte index of one lobus (n=15). Representative *Su(H)^{gwt}* lymph glands
1070 after wasp infestation are shown, co-stained for nuclear Pzg (in blue). Scale bars 100 µm.
1071 Statistical analyses with unpaired Student's t-test; only significant differences are indicated
1072 (*** $p<0.001$). (A-F) Representative images for each genotype and condition are shown in
1073 supplemental Figure 2.

1074 **(G)** qRT-PCR analyses measuring expression of NRE-GFP (left panel) and *atilla* (right
1075 panel). Transcript levels were quantified from hemolymph isolated from infested larvae at 0-6
1076 h or 24-30 h post-infestation as indicated, relative to the untreated *Su(H)^{gwt}* control. *Tbp* and
1077 *cyp33* served as reference genes. Shown data were gained from four biological and two
1078 technical replicates each. Left panel: Immediately after wasp infection, NRE-GFP expression
1079 dropped significantly in the *Su(H)^{gwt}* control, and even further to about 30% 24-30 h post-
1080 infection, whereas it remained at 60%-70% in the infested *Su(H)^{S269A}* mutants. Right panel:
1081 *atilla* transcripts remained stable at first in the *Su(H)^{gwt}* control, to rise dramatically 24-30 h
1082 post-infection, in contrast to *Su(H)^{S269A}*. Mini-max depicts 95% confidence, mean corresponds

1083 to expression ratio. Exact p-values are given in the raw data table. Significance was tested
1084 using PFRR from REST (*$p<0.05$).

1085 **Figure 2**

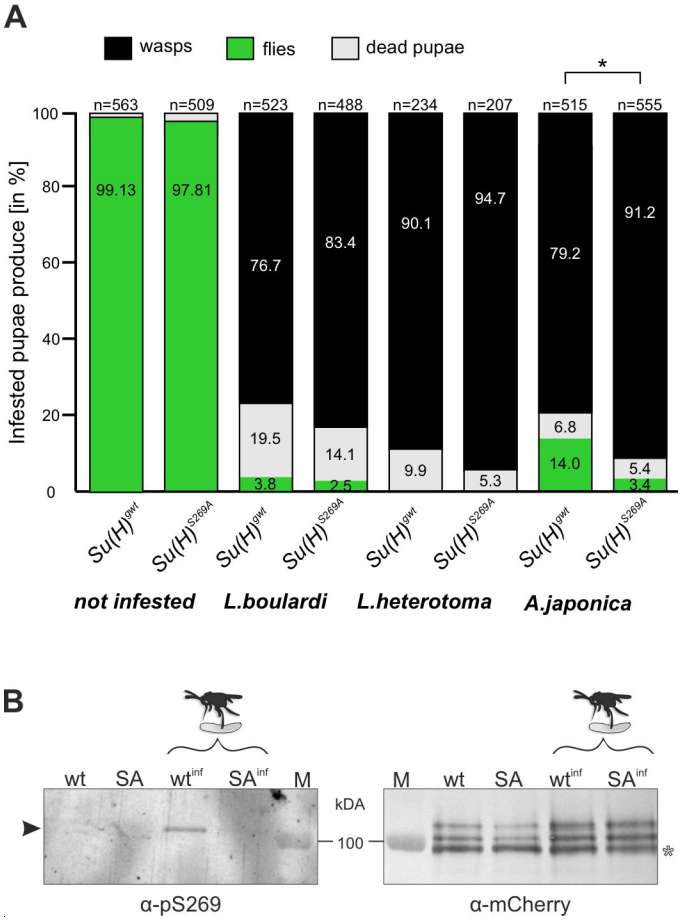

1086

1087

1088 ***Figure 2 Resistance to wasp infestation and phosphorylation at S269***

1089 **(A)** Resistance of *Su(H)*^{gwt} and *Su(H)*^{S269A} to the infestation with parasitic wasp strains *L.*
1090 *boulardi* and *L. heterotoma* (both family Figitidae) and *A. japonica* (family Braconidae), as
1091 indicated. Numbers of eclosed flies versus wasps as well as of dead pupae are presented in
1092 relation to the total of infested pupae. Left two columns are from non-infested controls. At
1093 least three independent experiments were performed, n=number of infested pupae.
1094 Statistically significant difference determined by Student's t-test is indicated with *$p<0.05$.
1095 **(B)** Su(H) is phosphorylated at Serine 269 upon parasitoid wasp infestation. Protein extracts
1096 from *Su(H)*$^{gwt\text{-}mCh}$ (wt) and *Su(H)*$^{S269A\text{-}mCh}$ (SA) larvae, respectively, infested (wt^{inf}, SA^{inf}) with
1097 *L. boulardi* or uninfested, were isolated by RFP-Trap precipitation and probed in Western
1098 blots. The anti-pS269 antiserum specifically detects wild type Su(H) protein only in wasp
1099 infested larvae (arrowhead), but not the Su(H)^{S269A} isoform. The blot on the right served as
1100 loading control, probed with anti-mCherry antibodies, revealing the typical Su(H) protein
1101 pattern in all lanes; the lowest band presumably stems from degradation (open asterisk). M,
1102 prestained protein ladder, protein size is given in kDa.

1103 **Figure 3**

1104

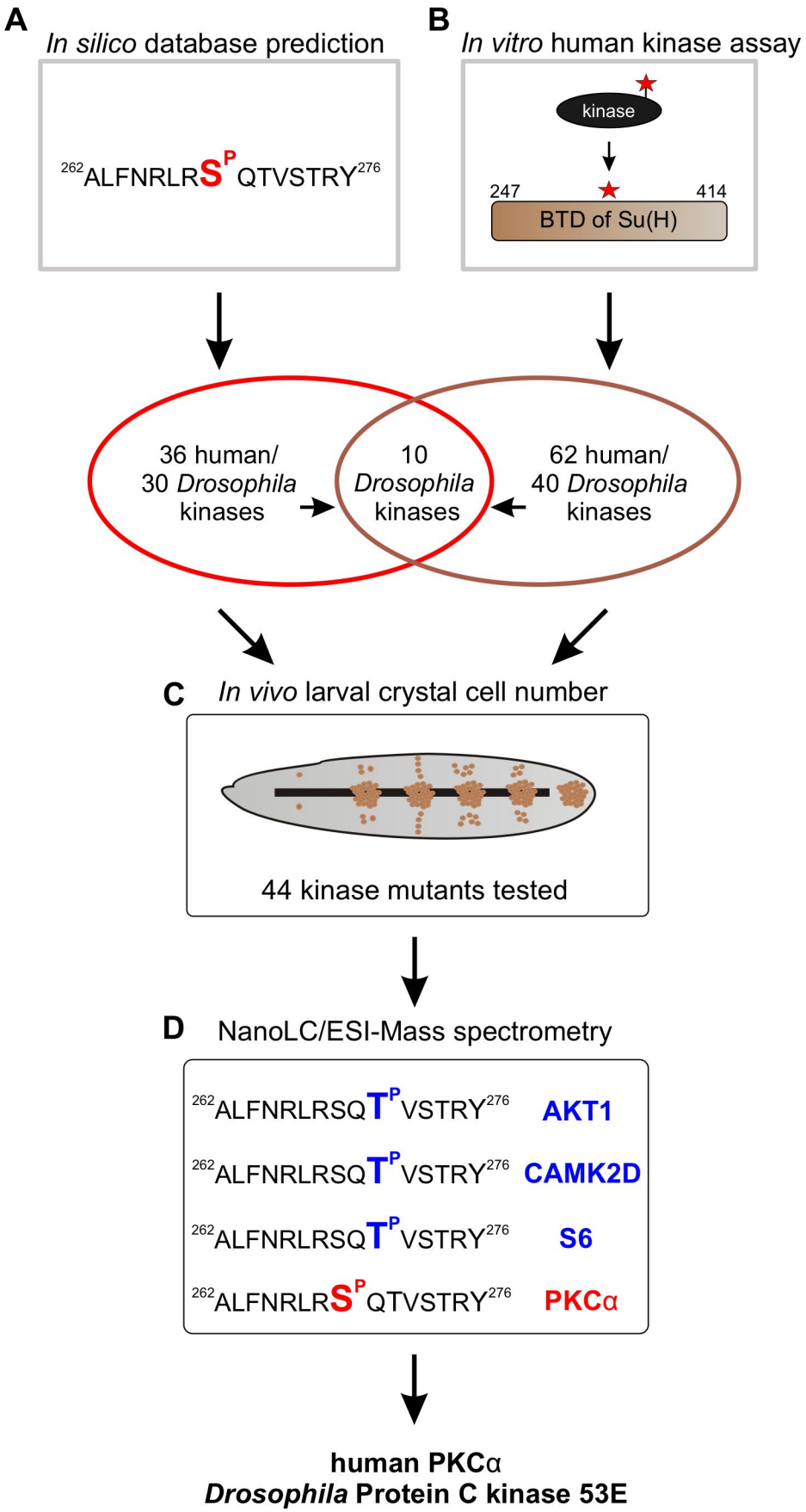

1105

1106 ***Figure 3 Pipeline of screening procedures for kinase candidates triggering phosphorylation***
1107 ***at Su(H)^{S269}***
1108 (**A**) *In silico* screening of database(s) predicting kinase recognition motif in Su(H)^{S269}; see
1109 Table 1 supplement. (**B**) *In vitro* assay screening 245 human Ser/Thr kinases for their ability
1110 to phosphorylate the BTD domain of Su(H); see Table 2 supplement. **(C)** *In vivo* screen of 44
1111 different *Drosophila* kinase mutants for crystal cell occurrence in third instar larvae; see
1112 Table 4 supplement. **(D)** NanoLC/ESI mass spectrometry with active human kinases
1113 monitoring their ability to phosphorylate the given Su(H) peptide. PKCα phosphorylates
1114 S269, whereas AKT1, CAMK2D and S6 kinase prefer T271. Spectra are shown in Figure 3_
1115 supplement 2.

1116 **Figure 4**

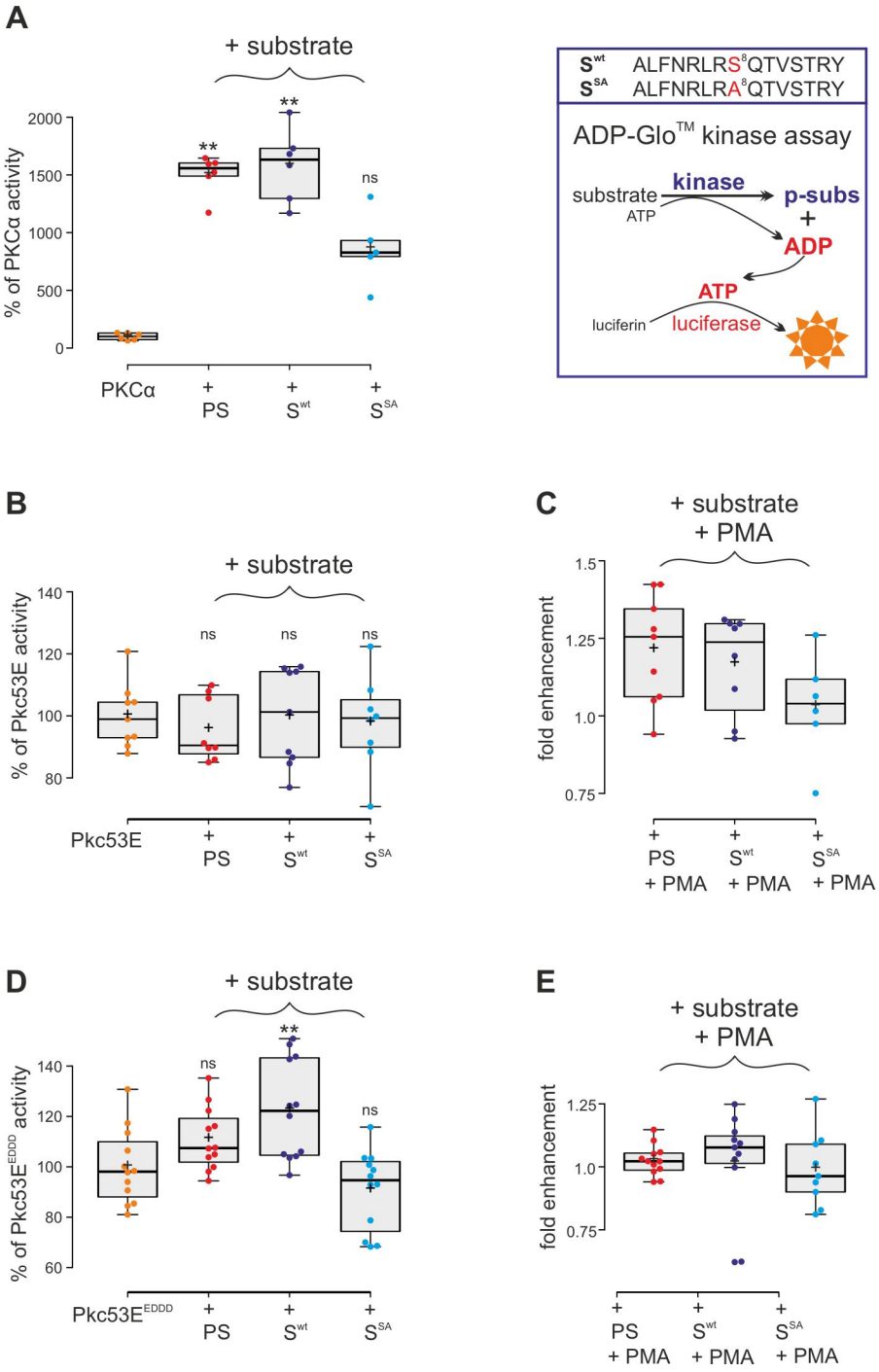

1117

1118

1119 ***Figure 4 Kinase assays using activated PKCα and Drosophila Pkc53E variants***

1120 (**A**) Right, schema of ADP-Glo™ assay to quantify kinase activity. The wild type (S^{wt}) and
1121 mutant (S^{SA}) Su(H) peptides 262-276 offered as specific kinase substrates are indicated
1122 above. Left, the commercially available, active human PKCα very efficiently phosphorylates
1123 the pseudo-substrate PS and the Su(H) S^{wt} peptide, but less efficiently the S^{SA} mutant peptide.
1124 Activity is given as percentage of the auto-active kinase without substrate. Each dot

represents one experiment. (**B**) Bacterially expressed Pkc53E has no activity on any of the offered substrates PS, S^{wt} or S^{SA}. (**C**) PMA raised Pkc53E activity to nearly 125% for PS and S^{wt} but not for S^{SA}. (**D**) Activated $Pkc53^{EDDD}$ phosphorylates PS and S^{wt} but not of S^{SA}. (**E**) Addition of PMA does not change $Pkc53^{EDDD}$ activity. Statistical analyses were performed with Kruskal-Wallis test followed by Dunn's test (A,C,E) or ANOVA followed by Tukey's approach in (B,D) with ** $p<0.01$, ns (not significant $p\geq0.05$).

1133 **Figure 5**

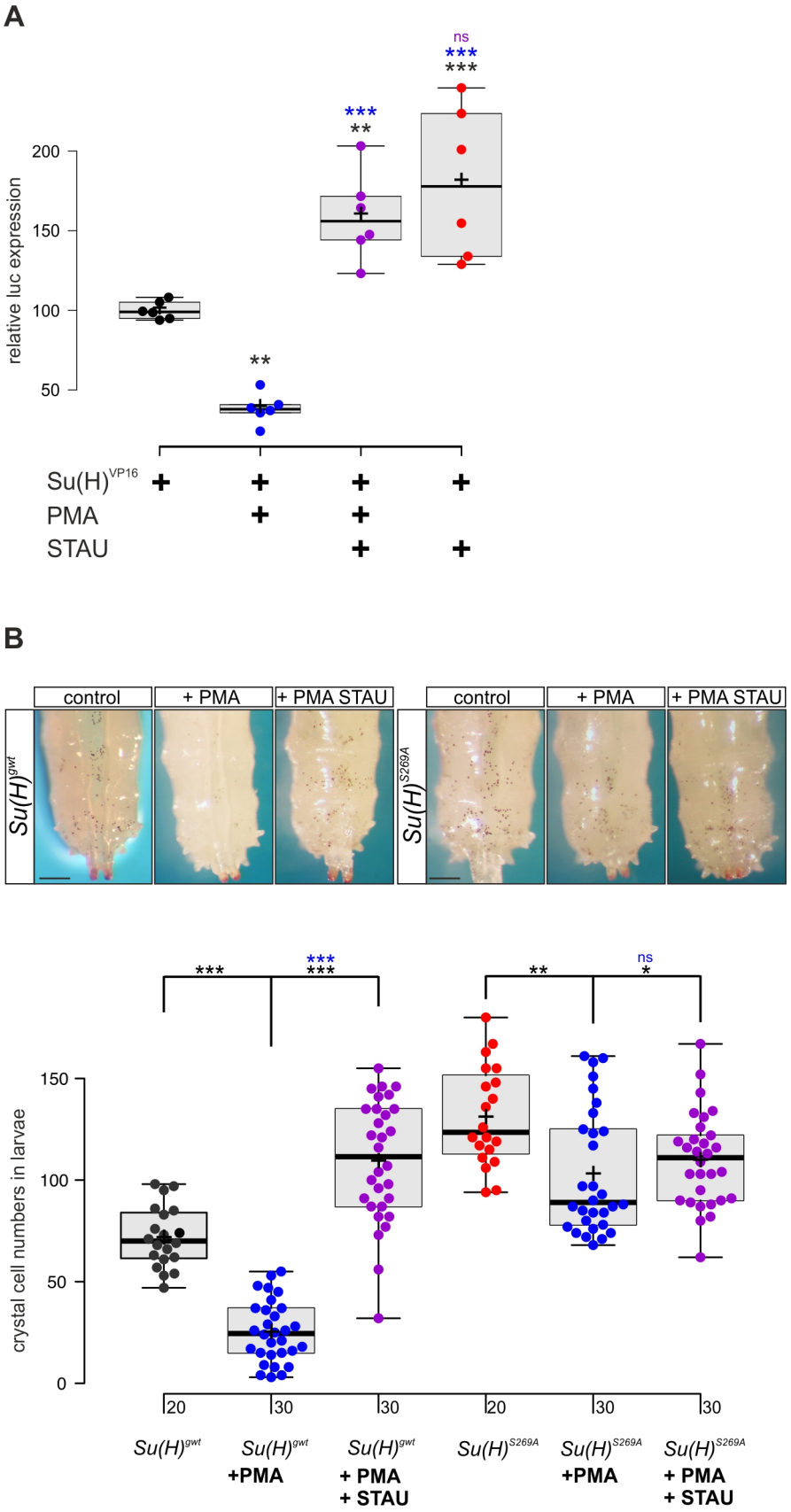

1134

1135

1136 ***Figure 5 PMA inhibits Su(H) transcriptional activity in vitro and crystal cell formation in***
1137 ***vivo***
1138 **(A)** Expression of NRE-luciferase reporter gene in *RBPj*^{ko} HeLa cells, transfected with
1139 2xMyc-Su(H)-VP16 [Su(H)^{VP16}]. Luciferase activity is given relative to the reporter construct
1140 normalized to Su(H)-VP16 set to 100%. Addition of PMA causes reduction of Su(H)-VP16
1141 dependent transcriptional activity to about 40%, which is reversed by the kinase inhibitor
1142 Staurosporine (STAU). STAU itself results in increased Su(H)-VP16 activity. Each dot
1143 represents one experiment (n=6). Statistical analysis was performed with ANOVA followed
1144 by Dunnet's multiple comparison test with *** $p<0.001$, ** $p<0.01$ relative to Su(H)-VP16
1145 alone (black asterisks) or to Su(H)-VP16 plus PMA (blue asterisks).
1146 **(B)** Number of melanized larval crystal cells determined in the last two segments of larvae fed
1147 with fly food plus 10% DMSO (control), or with fly food supplemented with 1mM PMA, or 1
1148 mM PMA plus 0.2 mM STAU (n=20 or 30 as indicated). Note strong drop of crystal cell
1149 numbers in the *Su(H)*^{gwt} control fed with PMA, and a reversal by STAU addition even above
1150 control levels. In contrast, PMA has a small effect on crystal cell number in the *Su(H)*^{S269A}
1151 mutant, which is reversed by STAU. Representative animals are shown above; scale bar 250
1152 µm. Statistical analysis was performed by ANOVA followed by Tukey's multiple comparison
1153 test (*** $p<0.001$), significant differences are colour coded.

1154 **Figure 6**

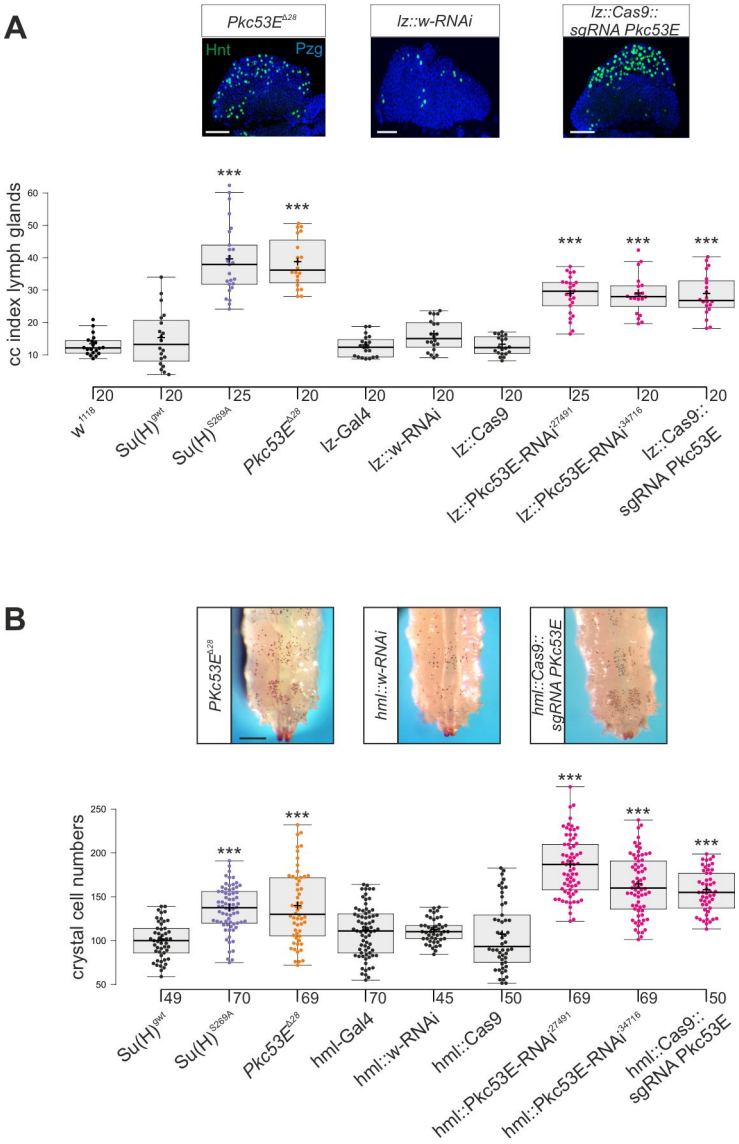

1155

1156 ***Figure 6 Loss of Pkc53E causes a gain of crystal cell number***

1157 Depletion of *Pkc53E* activity in the *Pkc53E*$^{\Delta 28}$ mutant or after knockdown by *Pkc53E*-RNAi
1158 or sg*Pkc53E* with the help of the Gal4-UAS system using *lz*-Gal4 (A) or *hml*-Gal4 (B).
1159 Controls as indicated. **(A)** Crystal cell index in lymph glands; each dot represents the value of
1160 an analysed lobus (n> 20 as indicated). Examples of *Pkc53E*$^{\Delta 28}$, *lz*::*Pkc53-RNAi* and *lz*::*Cas9*
1161 *sgPkc53E* are shown above. Crystal cells are labelled with Hnt (green), the lobe is stained
1162 with α-Pzg (blue). Scale bar 50 µm. Representative images of lymph glands for each
1163 genotype are shown in supplemental Figure S2A. Statistical analysis by ANOVA followed by
1164 Tukey's multiple comparison test relative to controls with *** p<0.001.
1165 **(B)** Melanized crystal cells enumerated from the last two segments of larvae with the given
1166 genotype (n=45-70 as indicated). Examples of respective *Pkc53E*$^{\Delta 28}$, *lz*::*Pkc53*-RNAi and
1167 *lz*::*Cas9 sgPkc53E* larvae are shown above. Scale bar 250 µm. Representative larval images

1168 for each genotype are shown in supplemental Figure S2B. Statistical analysis by Kruskal-
1169 Wallis test, followed by Dunn's test relative to controls with *** $p<0.001$. Note that there
1170 were no significant differences between any of the controls shown in black.

1171 **Figure 7**

1172

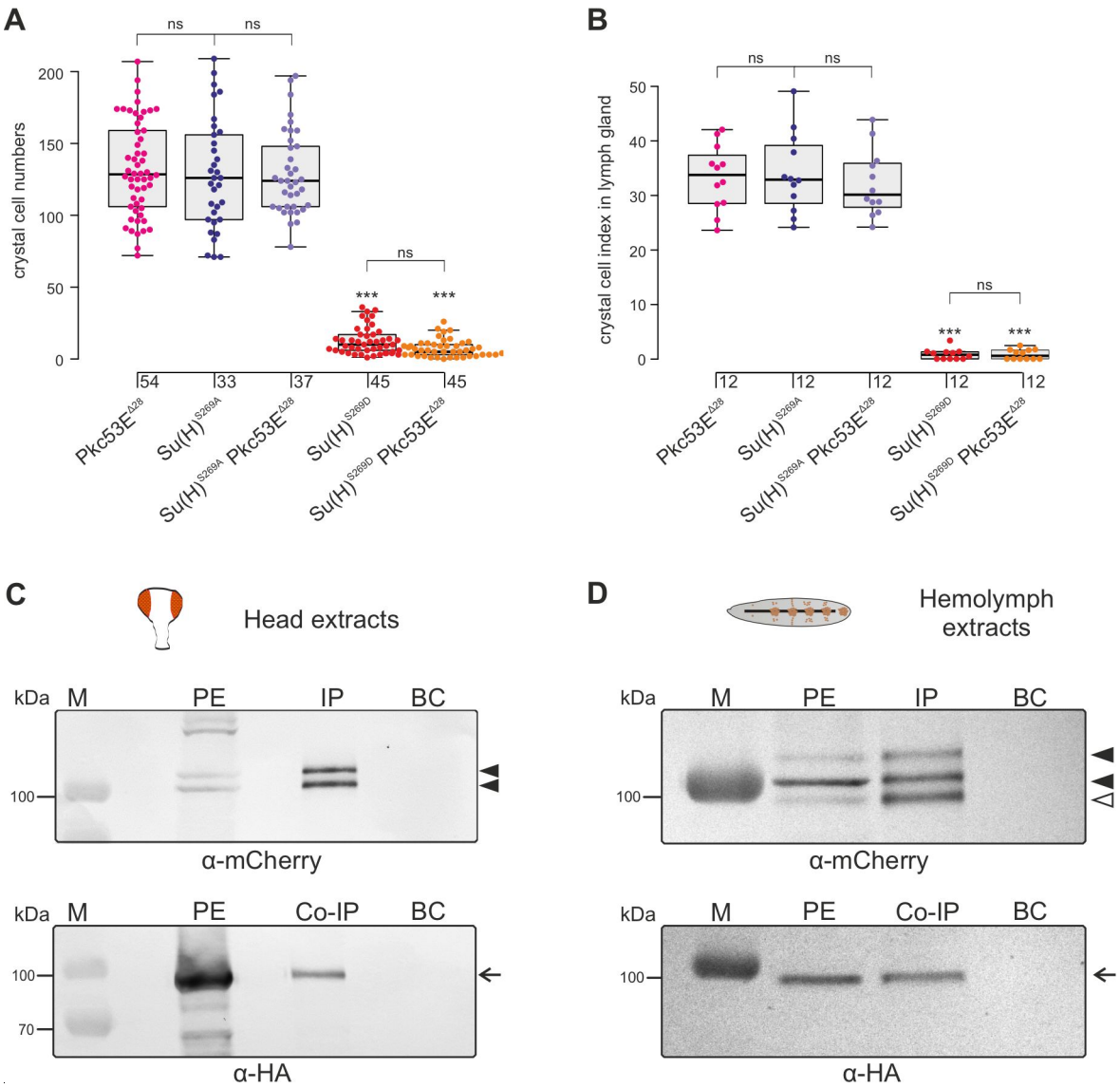

1173

1174

1175 ***Figure 7 Pkc53E interacts with Su(H) at a genetic and a physiological level***

1176 **(A)** Larval crystal cell numbers and **(B)** crystal cell indices in lymph glands were determined
1177 in the given genotypes. Each dot represents one analysed larva (n, as indicated) (A) or lymph
1178 gland lobus (n=12) (B Statistical analysis by Kruskal-Wallis test, followed by Dunn's test
1179 relative to controls with *** $p<0.001$; $p\geq0.05$ ns (not significant). Representative images of
1180 sessile crystal cells and of lymph glands for each genotype are shown in Figure supplement
1181 S1.

1182 (**C,D**) Co-immuno-precipitation of Pkc53E^{HA} with Su(H)$^{gwt\text{-}mCh}$ protein. RFP-Trap IP was
1183 performed with protein extracts from 400 heads (C) or 25 third instar larvae (D), respectively.
1184 UAS-Pkc53E-HA expression was induced with *Gmr*-Gal4 in the head or with *hml*-Gal4 in the

1185 hemolymph. Endogenous mCherry-tagged Su(H) was trapped and detected with anti-mCherry
1186 antibodies (black arrowheads). The lowest band from the hemolymph is presumably a
1187 degradation product (open arrowhead in (D)). HA-tagged Pkc53E was specifically co-
1188 precipitated as detected with anti-HA antibodies (arrow). 10% of the protein extract (PE) used
1189 for the IP-Trap was loaded for comparison. BC corresponds to the Trap with only agarose
1190 beads as a control. M, pre-stained protein ladder; protein size is given in kDa.
1191
1192
1193

1194 **Figure 8**

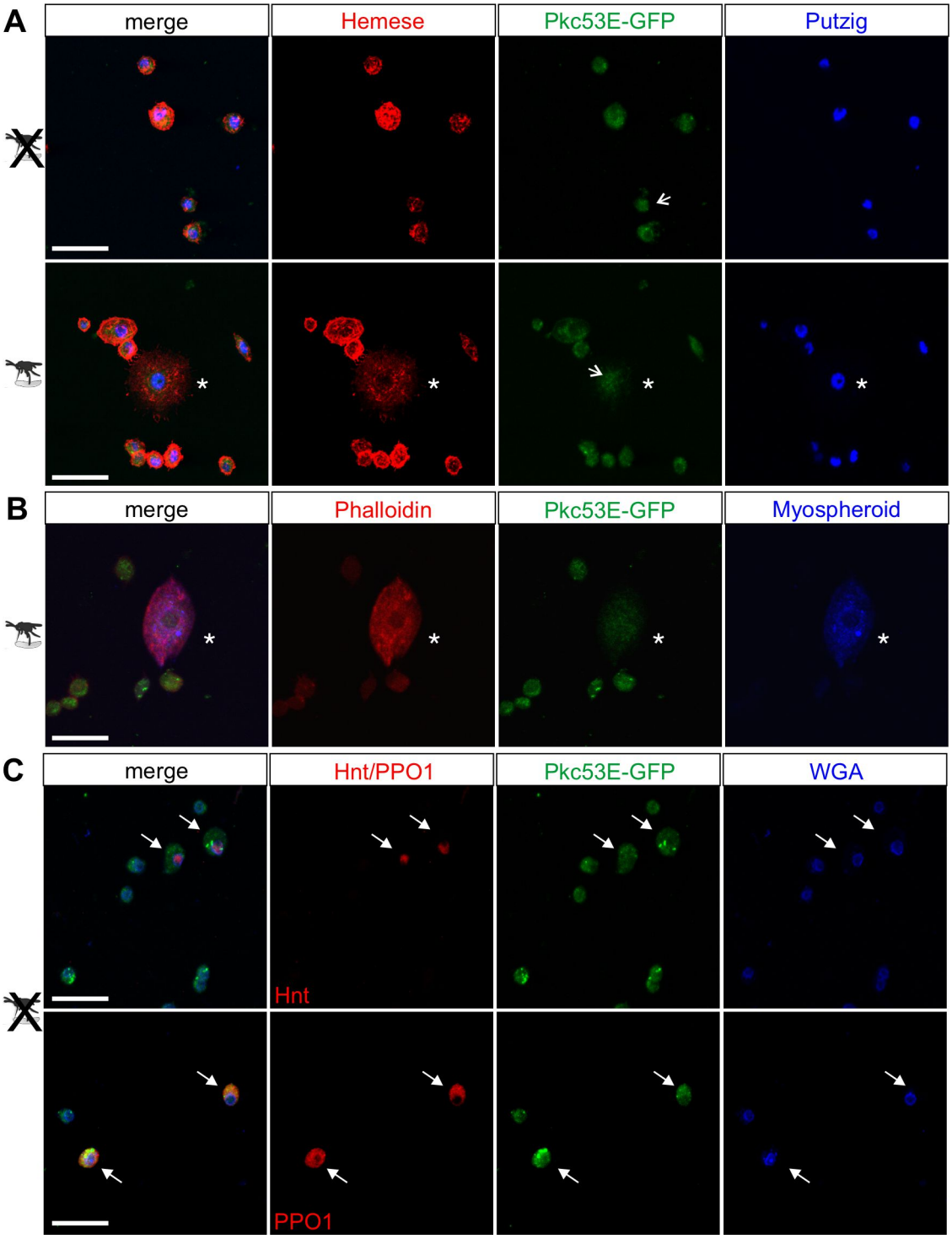

1195

1196 ***Figure 8 Pkc53E-eGFP is expressed in the cytoplasm of all hemocytes***

1197 Hemocytes derived from Pkc53E-eGFP expressing larvae, either infested or not infested with
1198 *L. boulardi* were stained with the antibodies and compounds indicated. GFP was detected
1199 directly without further antibody staining. **(A)** Pkc53E-eGFP is present in the cytoplasm of
1200 hemocytes independent of wasp infection. Note complete overlap with Hemese (red) marking
1201 all types of blood cells; Putzig (blue) labels nuclei. Asterisk denotes lamellocyte in

1202 hemolymph of infected larvae. Arrows point to nuclei expressing Pkc53E-eGFP. **(B)** Pkc53E-
1203 eGFP is expressed in the cytoplasm of a lamellocyte (asterisk), labelled with Myospheroid
1204 (blue) and Rhodamine-coupled Phalloidin (red). **(C)** Pkc53E-eGFP is enriched in the
1205 cytoplasm of crystal cells (arrow), labelled either with Hnt (red) or PPO1 (red), as indicated.
1206 Wheat germ agglutinin (WGA, blue) served to label nuclear lamina. Scale bar, 25 µm.
1207
1208

1209 **Figure 9**

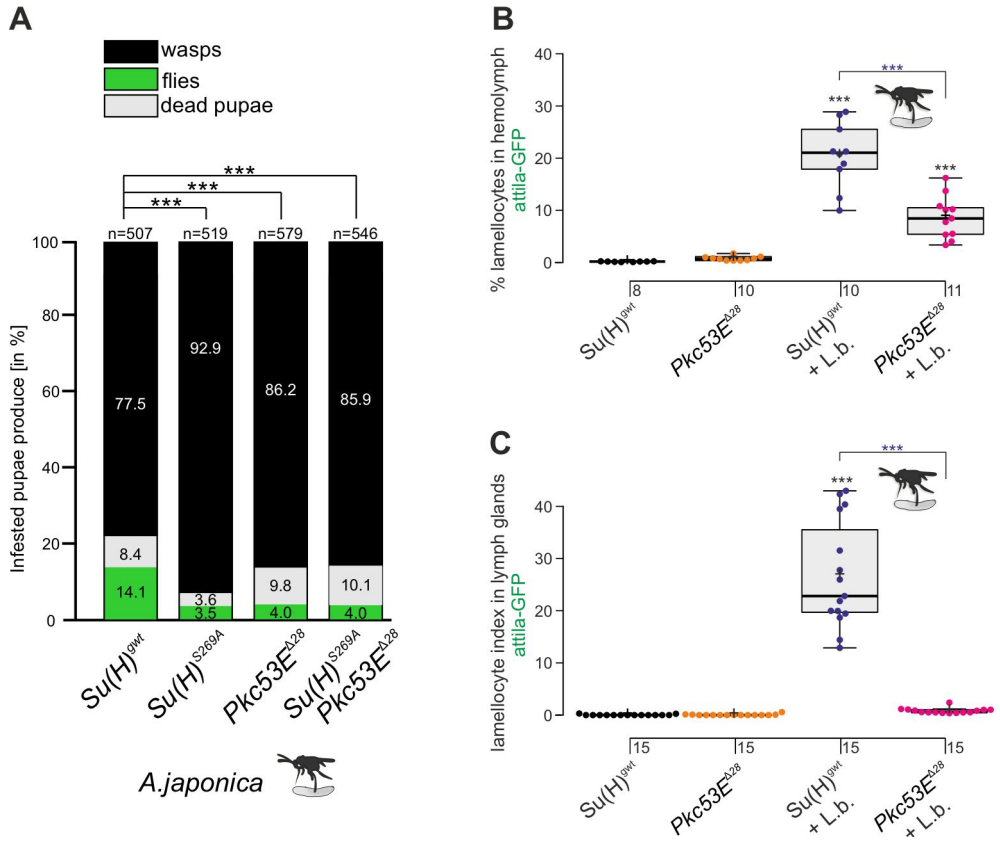

1210

1211

1212 ***Figure 9 The Pkc53E$^{\Delta 28}$ null mutant is immune compromised***

1213 **(A)** Resistance of *Pkc53E$^{\Delta 28}$* and the double mutant *Su(H)^{S269A} Pkc53E$^{\Delta 28}$*, compared to
1214 *Su(H)^{gwt}* and *Su(H)^{S269A}* for control, to the infestation with parasitic wasp strain *A. japonica*.
1215 Numbers of eclosed wasps versus flies as well as of dead pupae are presented in relation to
1216 the total of infested pupae (n, number of infested pupae). Statistical analysis by ANOVA
1217 followed by Tukey's multiple comparison test relative to control *Su(H)^{gwt}*; * $p<0.05$; ***
1218 $p<0.001$. **(B,C)** Quantification of lamellocytes labelled with the *atilla*-GFP reporter in the
1219 circulating hemolymph (B) or in the lymph glands (C), in un-infested conditions or upon
1220 wasp infestation as indicated. Representative images of hemolymph and of lymph glands for
1221 each genotype are shown in the supplement S2. (B) Fraction of GFP-positive lamellocytes
1222 relative to the total of DAPI-stained hemocytes in the pooled hemolymph from ten larvae.
1223 Each dot represents one larval pool (n, number of experiments as shown). (C) Lamellocyte
1224 index, i.e. number of GFP-labelled cells relative to the size of the lymph gland (n=15).
1225 Statistical analysis by ANOVA followed by Tukey's multiple comparison test; *** $p<0.001$;
1226 significant differences are colour coded.

1227

Additional information

Funding

This work was supported by a grant of the German Science Foundation DFG to ACN (NA 427/5-1) and by the University of Hohenheim. The funders had no role in study design, data collection and interpretation, or the decision to submit the work for publication.

Author contributions

Sebastian Deichsel, Data curation, Formal analysis, Methodology, Investigation, Resources, Writing—review and editing, Validation, Visualization; Lisa Frankenreiter, Formal analysis, Methodology, Investigation, Resources, Writing—review and editing, Validation; Johannes Fechner, Formal analysis, Methodology, Investigation, Resources, Writing—review and editing, Validation; Bernd M. Gahr, Data curation, Methodology, Investigation, Resources, Writing—review and editing, Visualization; Mirjam Zimmermann, Formal analysis, Investigation, Resources, Writing—review and editing; Helena Mastel, Investigation, Writing—review and editing; Irina Preis, Investigation, Writing—review and editing; Anette Preiss, Formal analysis, Writing—original draft, Writing—review and editing, Visualization; Anja C. Nagel, Conceptualization, Data curation, Formal analysis, Methodology, Writing—original draft, Writing—review and editing, Validation, Visualization, Supervision, Funding acquisition, Project administration.

Author ORCIDs

Bernd M. Gahr, https://orcid.org/0000-0002-5755-6603
Anette Preiss, https://orcid.org/0000-0002-6410-1586
Anja C. Nagel, https://orcid.org/0000-0002-2733-3249

Supplemental Materials

Figures Supplement

Figure 1 - Figure supplement 1

Notch acts upstream of Su(H); minor changes in hemocyte numbers in Su(H)^{S269} phospho-mutants

Figure 1 - Figure supplement 2

Representative images for the various settings

1262 **Figure 2 - Figure supplement 1**

1263 *The α-pS269 antiserum detects the phospho-mimetic Su(H) variant in vitro*

1264 **Figure 3 – Figure supplement 1**

1265 *Overview of the results from the kinase screen*

1266 **Figure 3 – Figure supplement 2**

1267 *MS/MS spectra of the phosphorylated Su(H) peptide*

1268 **Figure 4 – Figure supplement 1**

1269 *Conservation of Pkc53E and generation of an activated Pkc53E^{EDDD} isoform*

1270 **Figure 5 – Figure supplement 1**

1271 *Expression of Su(H)^{VP16}-myc is not influenced by PMA or STAU*

1272 **Figure 6 – Figure supplement 1**

1273 *The Pkc53E$^{\Delta 28}$ allele is a null mutant*

1274 **Figure 6 – Figure supplement 2**

1275 *Representative images for the various settings.*

1276 **Figure 7 – Figure supplement 1**

1277 *Representative images for the various settings.*

1278 **Figure 7 – Figure supplement 2**

1279 *Raw blots of co-IP*

1280 **Figure 8 – Figure supplement 1**

1281 *Pkc53E is expressed in hemocytes.*

1282 **Figure 9 – Figure supplement 1**

1283 *Pkc53E$^{\Delta 28}$ is sensitive to wasp infestation*

1284 **Figure 9 – Figure supplement 2**

1285 *Representative images for the various settings.*

1286

1287 **Tables Supplement**

1288 **Figure 3 – supplement Table 1**

1289 List of kinases predicted to recognize S269 in Su(H) as substrate *in silico*

1290 **Figure 3 – supplement Table 2**

1291 List of kinases accepting the BTD domain of Su(H) as substrate *in vitro*

1292 **Figure 3 – supplement Table 3**

1293 Fly strains used for the larval crystal cell screen

1294 **Figure 3 – supplement Table 4**

1295 Larval crystal cell screen

Supplemental Tables, Materials and Methods

S1 Table Key resources

S2 Table Oligonucleotides

Source data

Figure 1 source data

Raw data and statistical analysis

Figure 2 source data

Raw data and statistical analysis

Figure 4 source data

Raw data and statistical analysis

Figure 6 source data

Raw data and statistical analysis

Figure 7 source data

Raw data and statistical analysis

Figure 9 source data

Raw data and statistical analysis

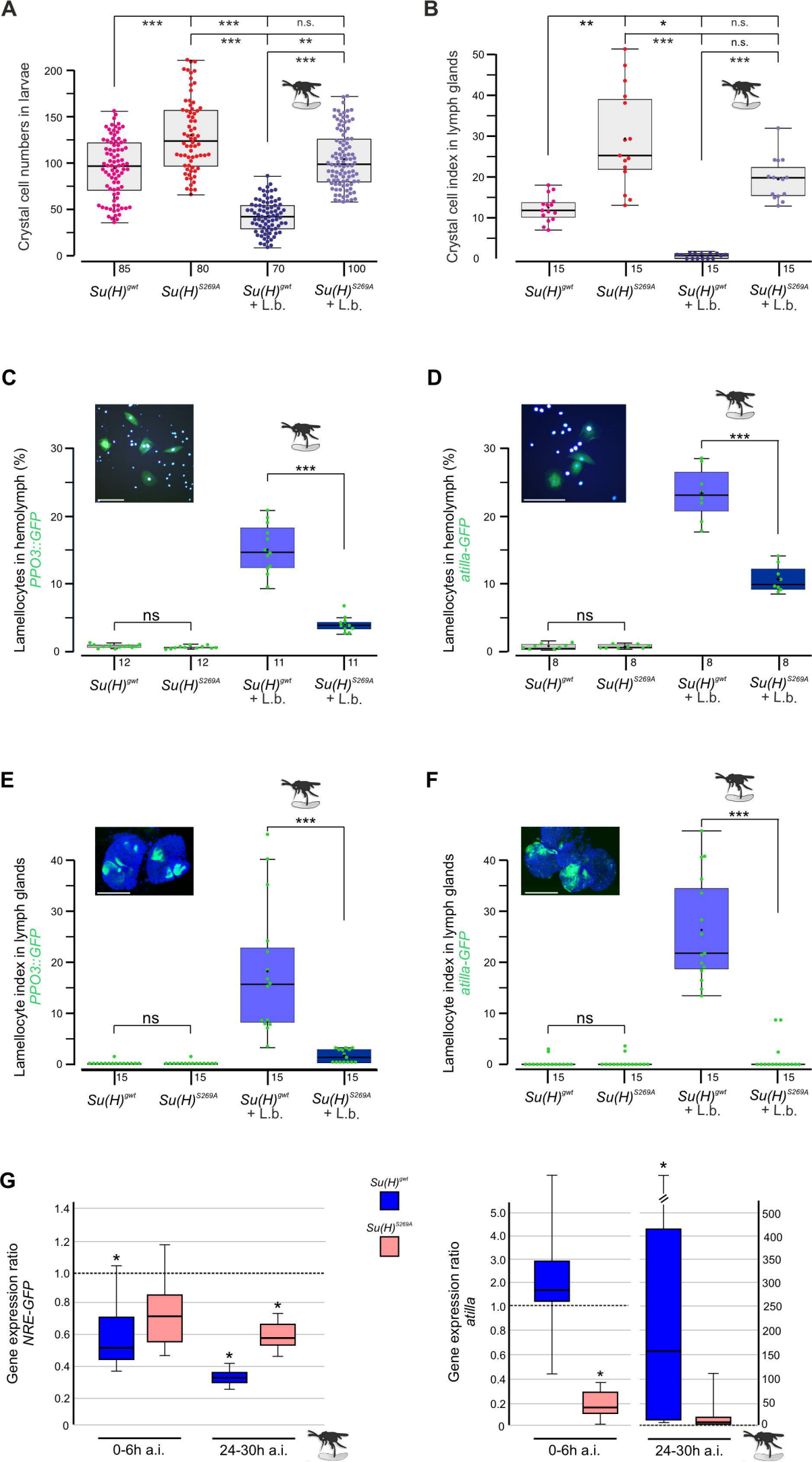
A
Crystal cell numbers in larvae
***
***
n.s.
***
**
***
85
80
70
100
Su(H)gwt
Su(H)S269A
Su(H)gwt + L.b.
Su(H)S269A + L.b.
B
Crystal cell index in lymph glands
**
*
n.s.
***
n.s.
***
15
15
15
15
C
Lamellocytes in hemolymph (%)
PPO3::GFP
***
ns
12
12
11
11
D
Lamellocytes in hemolymph (%)
atilla-GFP
***
ns
8
8
8
8
E
Lamellocyte index in lymph glands
PPO3::GFP
***
ns
15
15
15
15
F
Lamellocyte index in lymph glands
atilla-GFP
***
ns
15
15
15
15
G
Gene expression ratio
NRE-GFP
0-6h a.i.
24-30h a.i.
Gene expression ratio
atilla
0-6h a.i.
24-30h a.i.

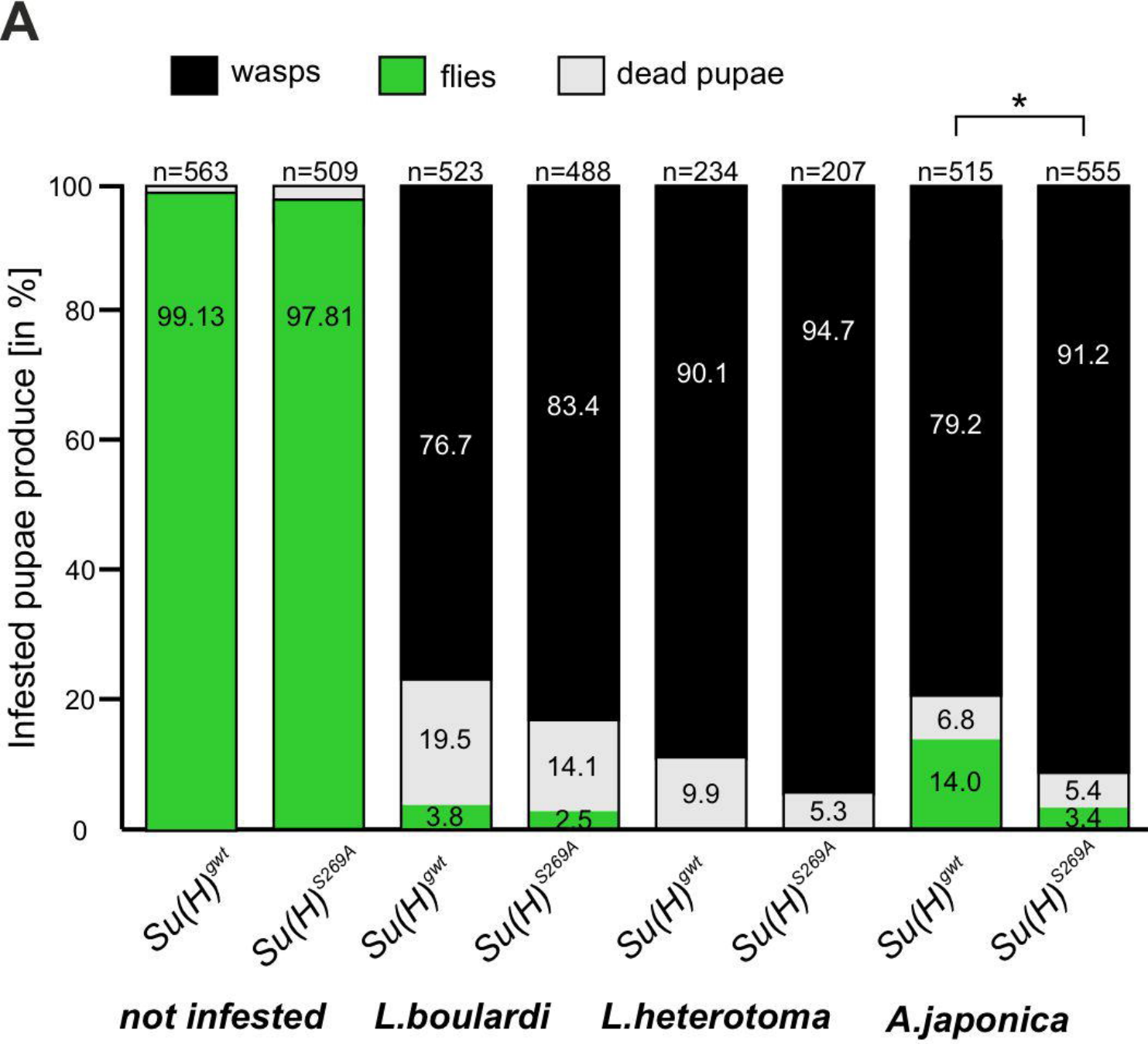
A
wasps
flies
dead pupae
*
n=563
n=509
n=523
n=488
n=234
n=207
n=515
n=555
Infested pupae produce [in %]
100
80
60
40
20
0
99.13
97.81
76.7
19.5
3.8
83.4
14.1
2.5
90.1
9.9
94.7
5.3
79.2
6.8
14.0
91.2
5.4
3.4
Su(H)gwt
Su(H)S269A
not infested
L.boulardi
L.heterotoma
A.japonica

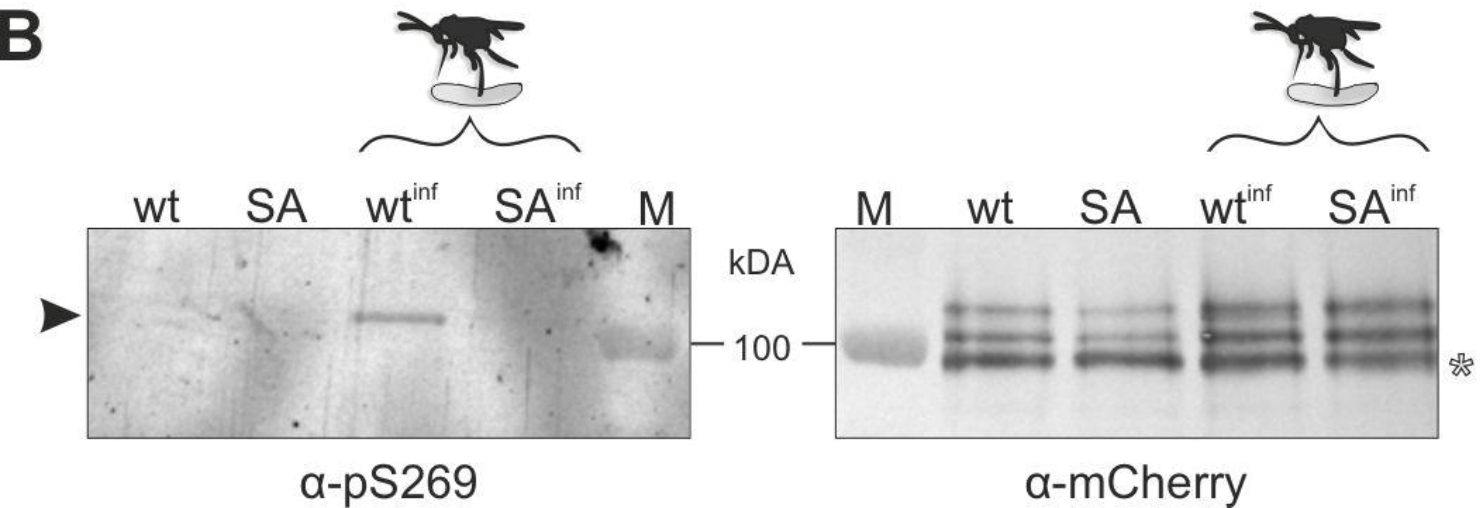
B
wt
SA
wtinf
SAinf
M
kDA
100
α-pS269
α-mCherry

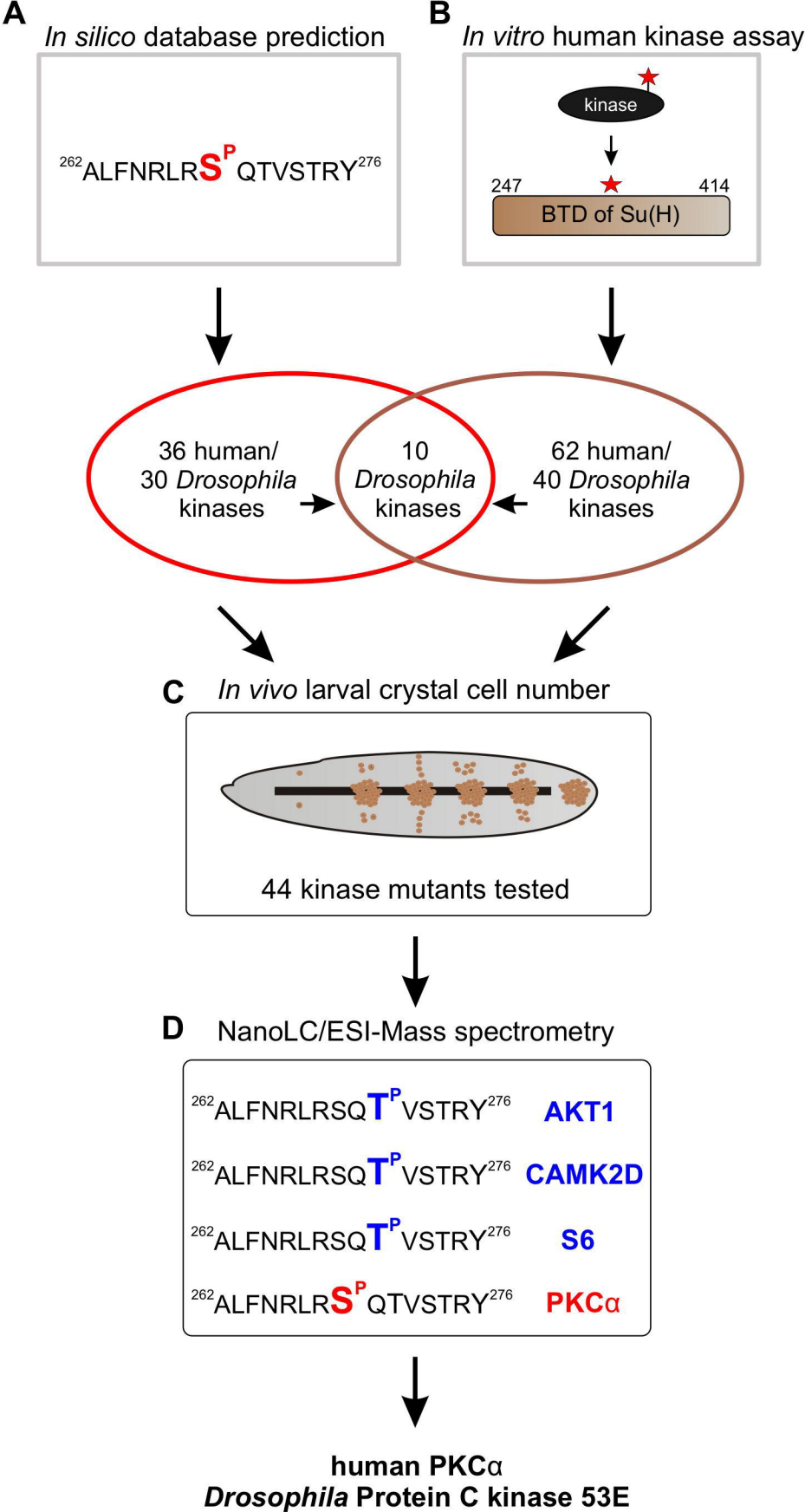
A
In silico database prediction
262ALFNRLRSPQTVSTRY276
B
In vitro human kinase assay
kinase
247
414
BTD of Su(H)
36 human/
30 Drosophila
kinases
10
Drosophila
kinases
62 human/
40 Drosophila
kinases
C
In vivo larval crystal cell number
44 kinase mutants tested
D
NanoLC/ESI-Mass spectrometry
262ALFNRLRSQTPVSTRY276
AKT1
262ALFNRLRSQTPVSTRY276
CAMK2D
262ALFNRLRSQTPVSTRY276
S6
262ALFNRLRSPQTVSTRY276
PKCα
human PKCα
Drosophila Protein C kinase 53E

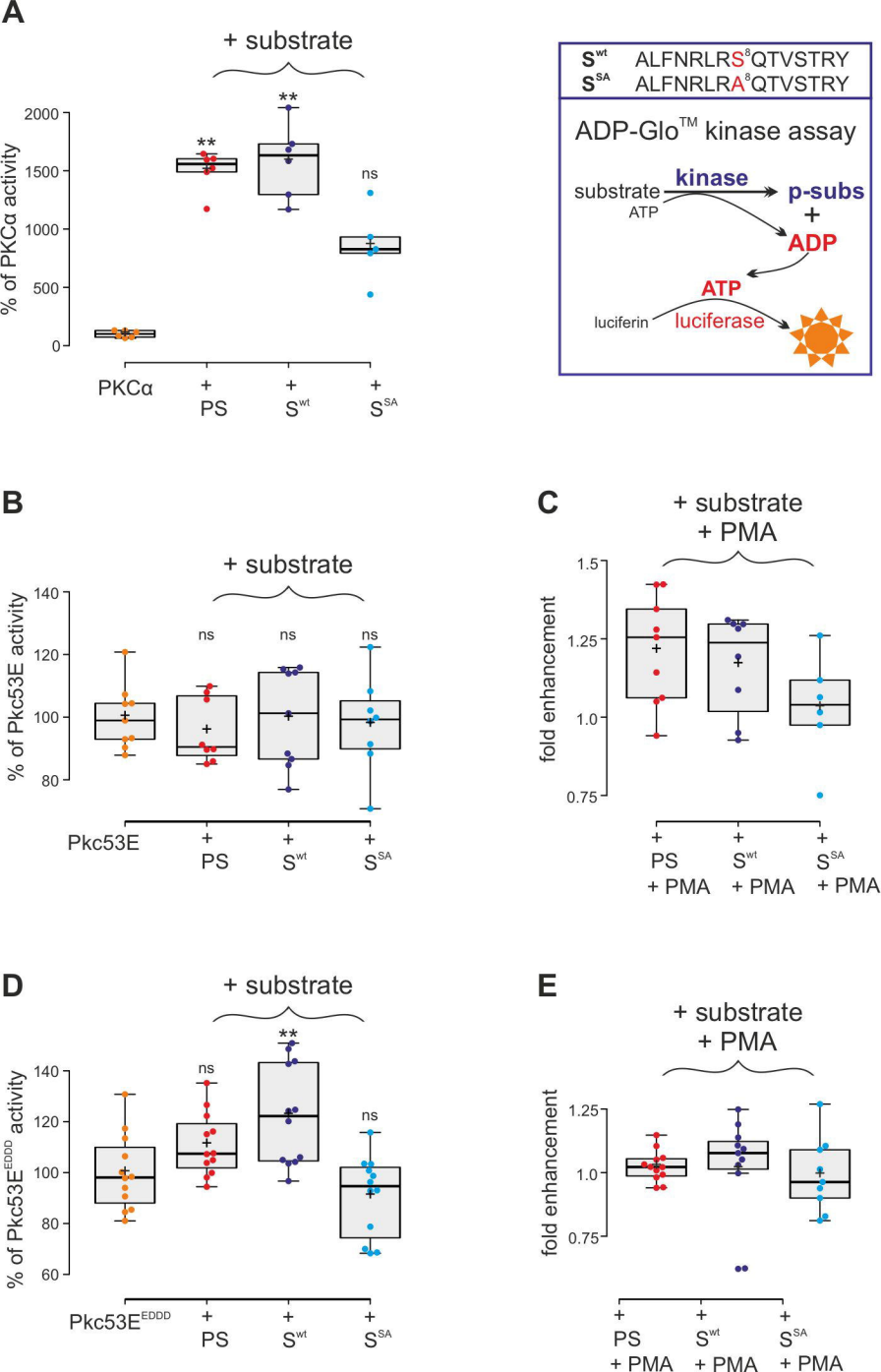
A
+ substrate
% of PKCα activity
2000
1500
1000
500
0
**
**
ns
PKCα
+ PS
+ S^wt
+ S^SA
S^wt ALFNRLRS^8QTVSTRY
S^SA ALFNRLRA^8QTVSTRY
ADP-Glo™ kinase assay
substrate
ATP
kinase
p-subs
+
ADP
ATP
luciferin
luciferase
B
+ substrate
% of Pkc53E activity
140
120
100
80
ns
ns
ns
Pkc53E
+ PS
+ S^wt
+ S^SA
C
+ substrate
+ PMA
fold enhancement
1.5
1.25
1.0
0.75
+ PS + PMA
+ S^wt + PMA
+ S^SA + PMA
D
+ substrate
% of Pkc53E^EDDD activity
140
120
100
80
60
ns
**
ns
Pkc53E^EDDD
+ PS
+ S^wt
+ S^SA
E
+ substrate
+ PMA
fold enhancement
1.25
1.0
0.75
+ PS + PMA
+ S^wt + PMA
+ S^SA + PMA

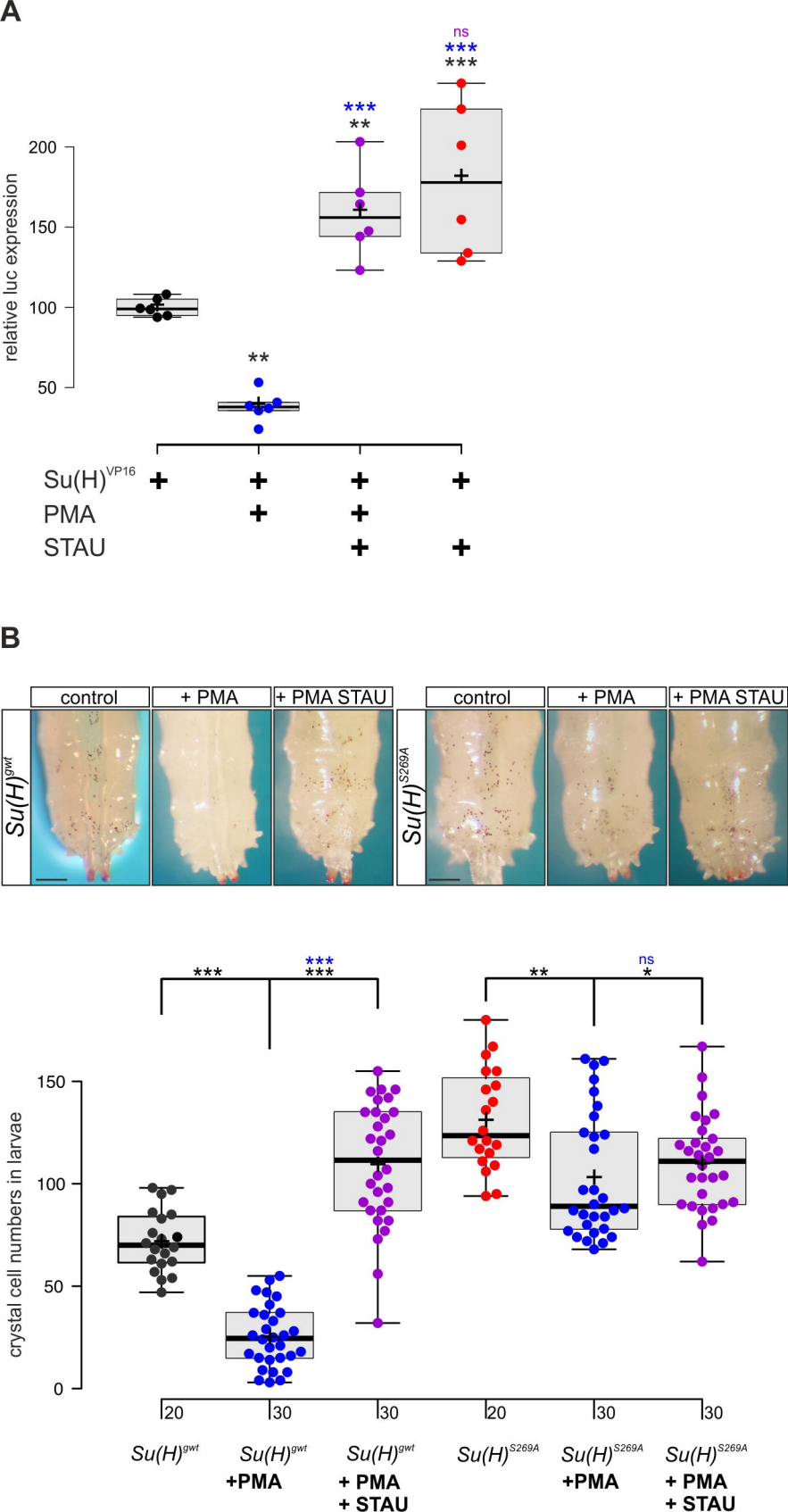
A
relative luc expression
200
150
100
50
ns
***
***
***
**
**
Su(H)VP16
PMA
STAU
B
control
+ PMA
+ PMA STAU
Su(H)gwt
Su(H)S269A
crystal cell numbers in larvae
150
100
50
0
***
***
***
**
ns
*
20
30
30
20
30
30
Su(H)gwt
Su(H)gwt +PMA
Su(H)gwt + PMA + STAU
Su(H)S269A
Su(H)S269A +PMA
Su(H)S269A + PMA + STAU

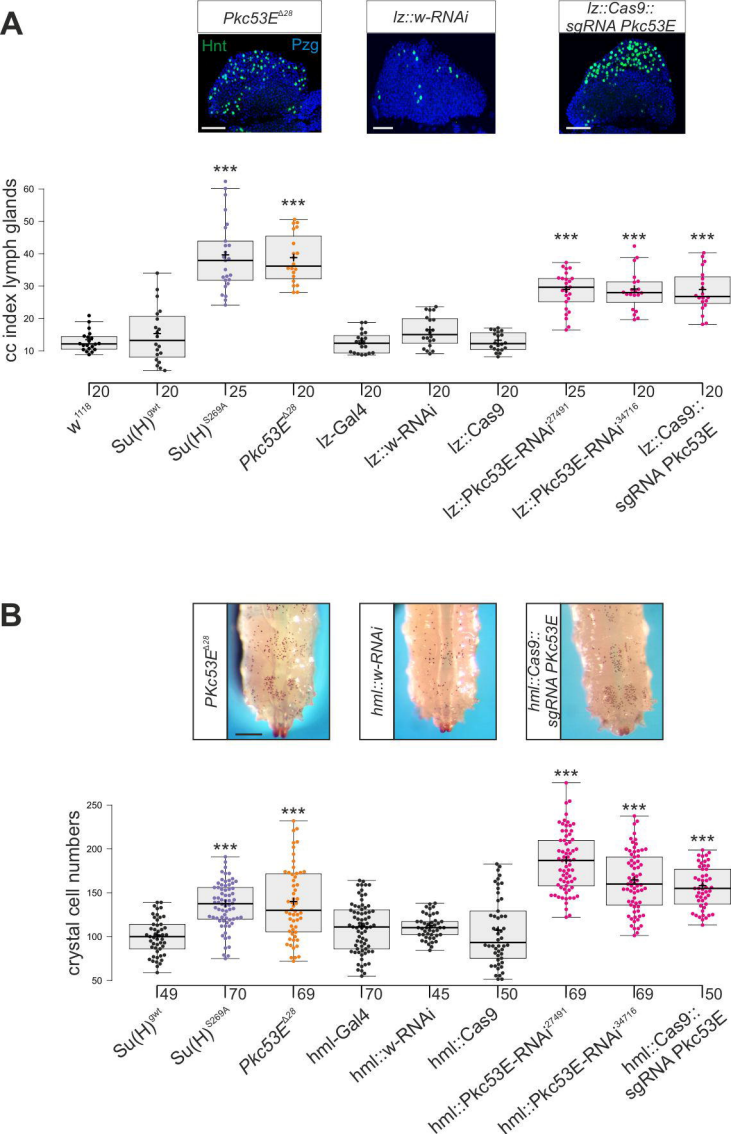
A
Pkc53E^Δ28
lz::w-RNAi
lz::Cas9::
sgRNA Pkc53E
Hnt
Pzg
cc index lymph glands
60
50
40
30
20
10
***
***
***
***
***
20
20
25
20
20
20
20
25
20
20
w^1118
Su(H)^PW1
Su(H)^S289A
Pkc53E^Δ28
lz-Gal4
lz::w-RNAi
lz::Cas9
lz::Pkc53E-RNAi^27491
lz::Pkc53E-RNAi^34716
lz::Cas9::
sgRNA Pkc53E
B
PKc53E^Δ28
hml::w-RNAi
hml::Cas9::
sgRNA PKc53E
crystal cell numbers
250
200
150
100
50
***
***
***
***
***
49
70
69
70
45
50
69
69
50
Su(H)^PW1
Su(H)^S289A
Pkc53E^Δ28
hml-Gal4
hml::w-RNAi
hml::Cas9
hml::Pkc53E-RNAi^27491
hml::Pkc53E-RNAi^34716
hml::Cas9::
sgRNA Pkc53E

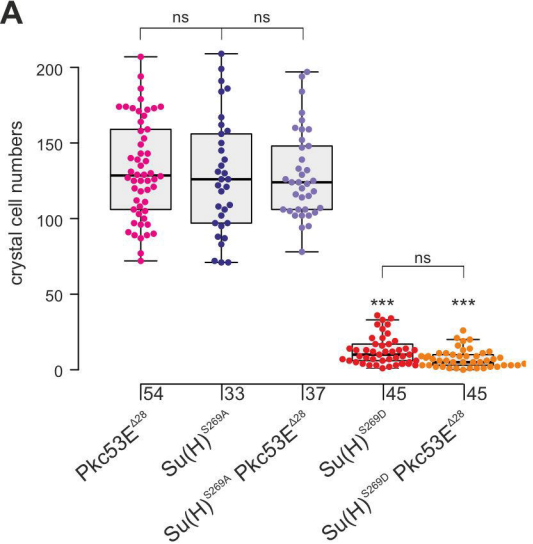
A
ns
ns
ns
***
***
crystal cell numbers
200
150
100
50
0
54
33
37
45
45
Pkc53E$^{\Delta 28}$
Su(H)^{S269A}
Su(H)^{S269A} Pkc53E$^{\Delta 28}$
Su(H)^{S269D}
Su(H)^{S269D} Pkc53E$^{\Delta 28}$

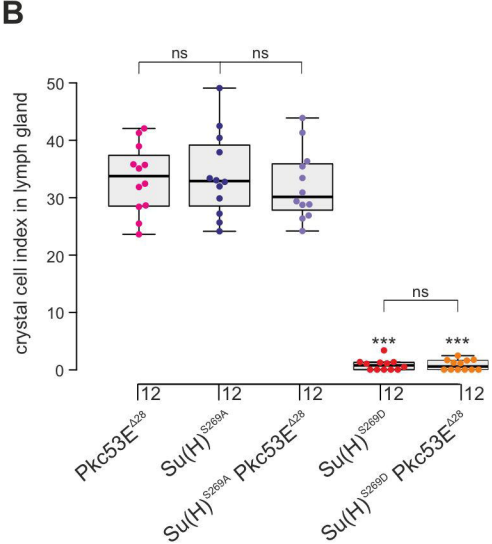
B
ns
ns
ns
***
***
crystal cell index in lymph gland
50
40
30
20
10
0
12
12
12
12
12
Pkc53E$^{\Delta 28}$
Su(H)^{S269A}
Su(H)^{S269A} Pkc53E$^{\Delta 28}$
Su(H)^{S269D}
Su(H)^{S269D} Pkc53E$^{\Delta 28}$

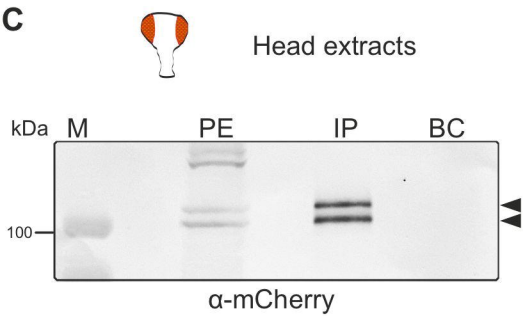
C
Head extracts
kDa
M
PE
IP
BC
100
α-mCherry

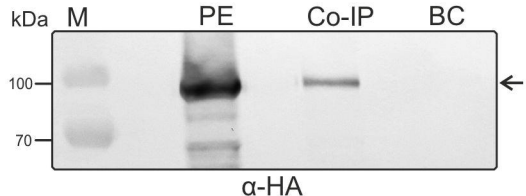
kDa
M
PE
Co-IP
BC
100
70
α-HA

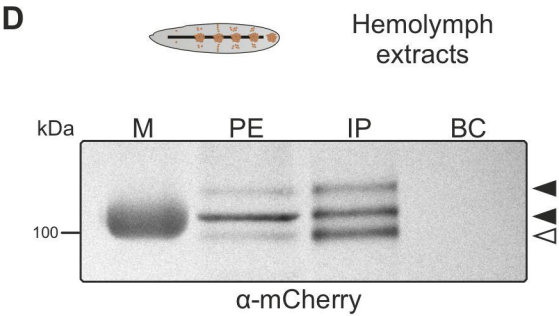
D
Hemolymph extracts
kDa
M
PE
IP
BC
100
α-mCherry

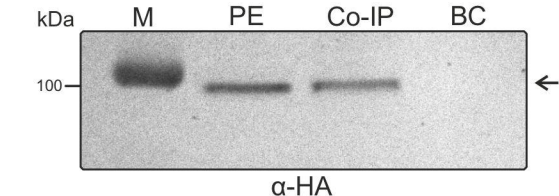
kDa
M
PE
Co-IP
BC
100
α-HA

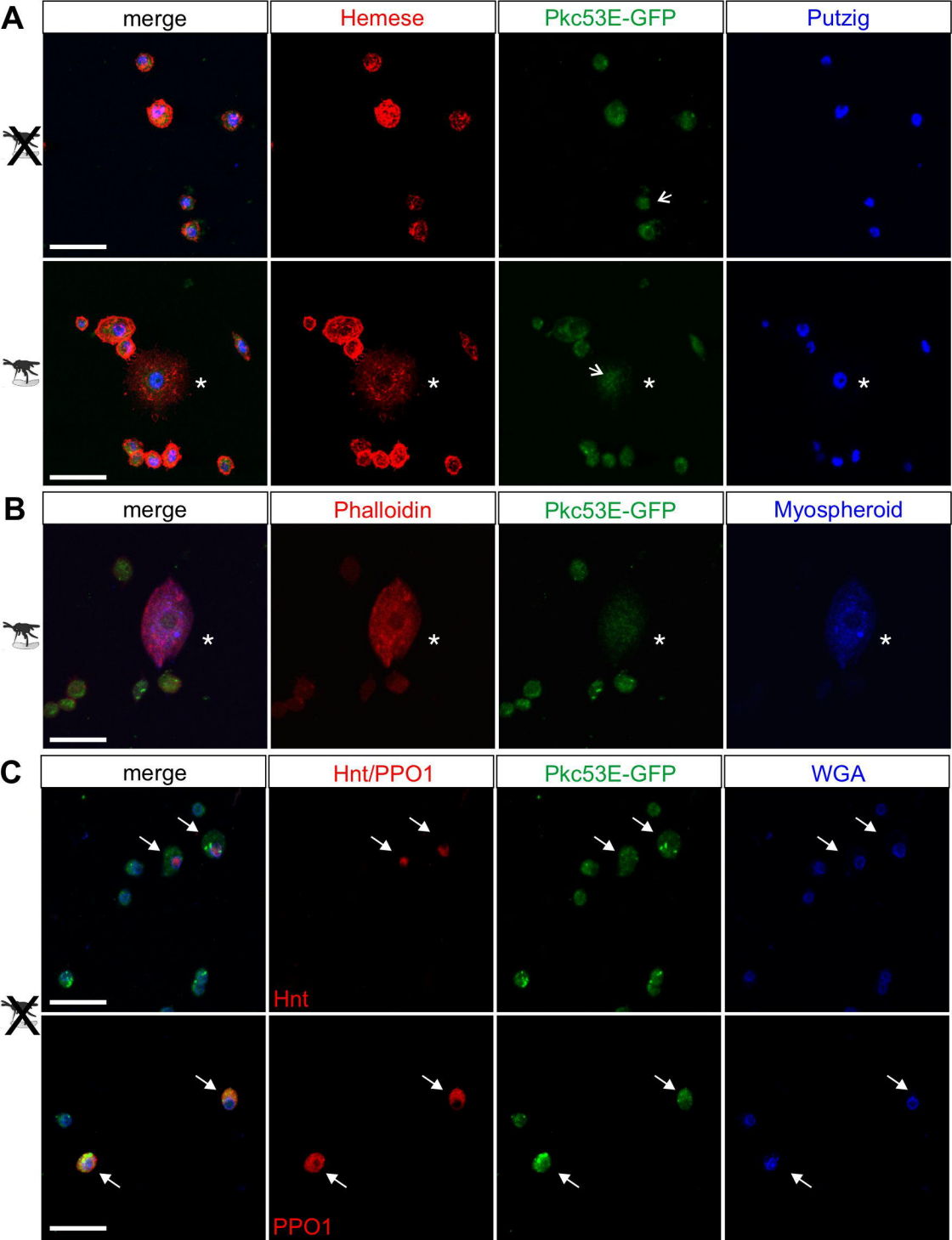
A
merge
Hemese
Pkc53E-GFP
Putzig
B
merge
Phalloidin
Pkc53E-GFP
Myospheroid
C
merge
Hnt/PPO1
Pkc53E-GFP
WGA
Hnt
PPO1

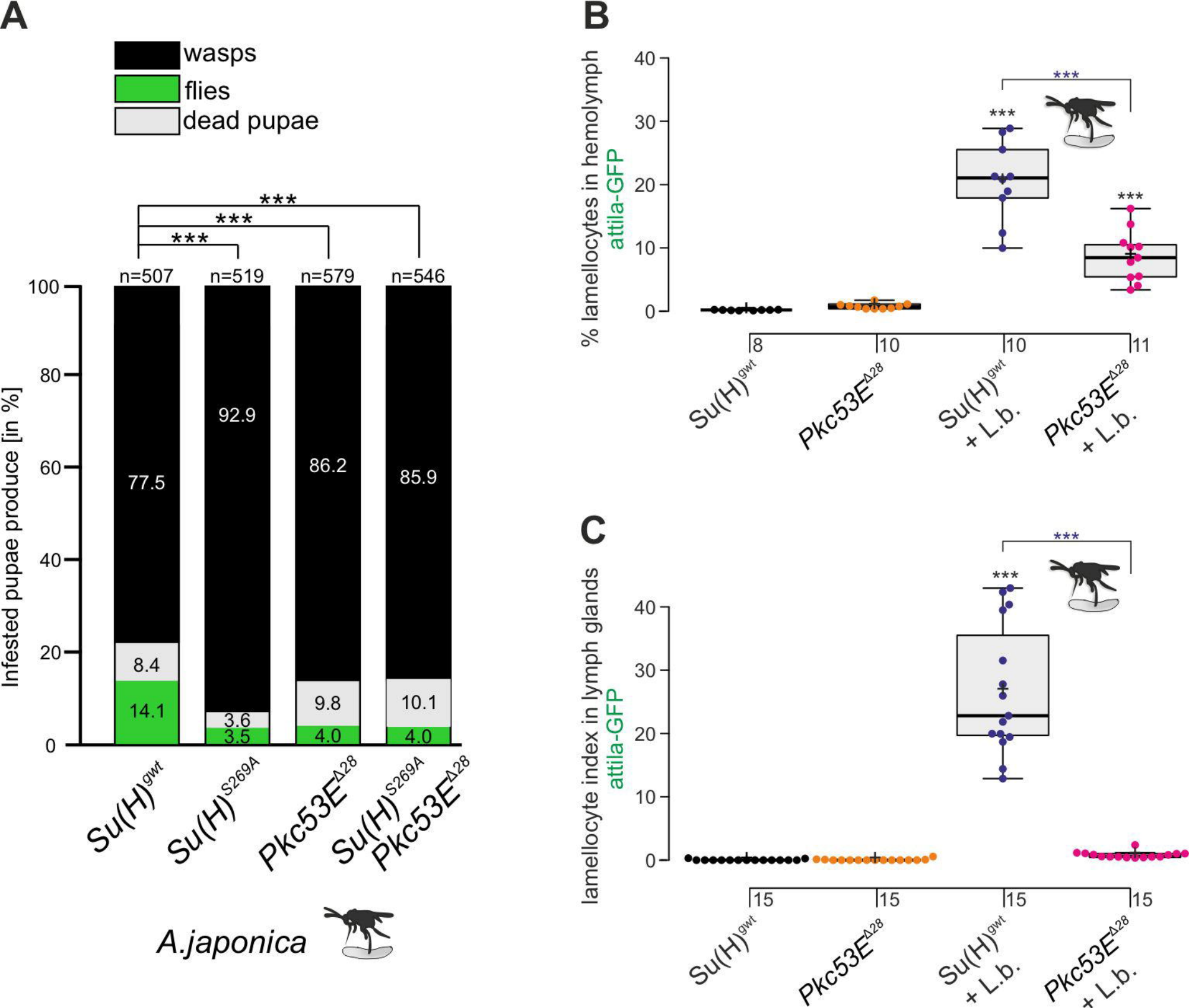
A
wasps
flies
dead pupae
***
***
***
n=507
n=519
n=579
n=546
Infested pupae produce [in %]
100
80
60
40
20
0
77.5
8.4
14.1
92.9
3.6
3.5
86.2
9.8
4.0
85.9
10.1
4.0
Su(H)gwt
Su(H)S269A
Pkc53EΔ28
Su(H)S269A Pkc53EΔ28
A.japonica
B
% lamellocytes in hemolymph
attila-GFP
40
30
20
10
0
***
***
***
8
10
10
11
Su(H)gwt
Pkc53EΔ28
Su(H)gwt + L.b.
Pkc53EΔ28 + L.b.
C
lamellocyte index in lymph glands
attila-GFP
40
30
20
10
0
***
***
15
15
15
15
Su(H)gwt
Pkc53EΔ28
Su(H)gwt + L.b.
Pkc53EΔ28 + L.b.